frontiers in Earth Science

ORIGINAL RESEARCH
published: 29 November 2019
doi: 10.3389/feart.2019.00316

Mg and Li Stable Isotope Ratios of Rocks, Minerals, and Water in an Outlet Glacier of the Greenland Ice Sheet

Ruth S. Hindshaw[1]*, *Jörg Rickli*[2] and *Julien Leuthold*[2]

[1] Department of Earth Sciences, University of Cambridge, Cambridge, United Kingdom, [2] Department of Earth Sciences, Institute of Geochemistry and Petrology, ETH Zurich, Zurich, Switzerland

Magnesium and lithium stable isotope ratios (δ^{26}Mg and δ^{7}Li) have shown promise as tools to elucidate biogeochemical processes both at catchment scales and in deciphering global climate processes. Nevertheless, the controls on riverine Mg and Li isotope ratios are often difficult to determine as a myriad of factors can cause fractionation from bulk rock values such as secondary mineral formation and preferential weathering of isotopically distinct mineral phases. Quantifying the relative contribution from carbonate and silicate minerals to the dissolved load of glacierized catchments is particularly crucial for determining the role of chemical weathering in modulating the carbon cycle over glacial-interglacial periods. In this study we report Mg and Li isotope data for water, river sediment, rock, and mineral separates from the Leverett Glacier catchment, West Greenland. We assess whether the silicate mineral contributions to the dissolved load, previously determined using radiogenic Sr, Ca, Nd, and Hf isotopes, are consistent with dissolved Mg and Li isotope data, or whether a carbonate contribution is required as inferred previously for this region. For δ^{7}Li, the average dissolved river water value ($+19.2 \pm 2.5$‰, 2SD) was higher than bedrock, river sediment, and mineral δ^{7}Li values, implying a fractionation process. For δ^{26}Mg, the average dissolved river water value (-0.30 ± 0.14‰, 2SD) was within error of bedrock and river sediment and within the range of mineral δ^{26}Mg values (-1.63 to $+0.06$‰). The river δ^{26}Mg values are consistent with the mixing of Mg derived from the same mineral phases previously identified from radiogenic isotope measurements as controlling the dissolved load chemistry. Glacier fed rivers previously measured in this region had δ^{26}Mg values ~0.80‰ lower than those measured in the Leverett River which could be caused by a larger contribution from garnet (-1.63‰) dissolution compared to Leverett. This study highlights that dissolved Mg and Li isotope ratios in the Leverett River are affected by different processes (mixing and fractionation), and that since variations in silicate mineral δ^{26}Mg values exist, preferential weathering of individual silicate minerals should be considered in addition to carbonate when interpreting dissolved δ^{26}Mg values.

Keywords: chemical weathering, Leverett glacier, mineral separates, silicate, Li isotopes, Mg isotopes

OPEN ACCESS

Edited by:
Sophie Opfergelt, Catholic University of Louvain, Belgium

Reviewed by:
Anne-Sophie Bouvier, Université de Lausanne, Switzerland
Jacob Clement Yde, Western Norway University of Applied Sciences, Norway
Christopher Robert Pearce, University of Southampton, United Kingdom

***Correspondence:**
Ruth S. Hindshaw
ruth.hindshaw@gmail.com

Specialty section:
This article was submitted to Geochemistry, a section of the journal Frontiers in Earth Science

Received: *18 August 2019*
Accepted: *14 November 2019*
Published: *29 November 2019*

Citation:
Hindshaw RS, Rickli J and Leuthold J (2019) Mg and Li Stable Isotope Ratios of Rocks, Minerals, and Water in an Outlet Glacier of the Greenland Ice Sheet. Front. Earth Sci. 7:316. doi: 10.3389/feart.2019.00316

1. INTRODUCTION

Chemical weathering in glacierized regions results in water with a chemical composition distinct to that originating from non-glacierized regions (e.g., Tranter, 2003). Glacial erosion produces fine grained sediments that, combined with high discharge conditions during the melt season, leads to the preferential weathering of mineral phases such as calcite, sulfide, and biotite, resulting in elevated Ca and K concentrations (Anderson et al., 1997; Blum and Erel, 1997; Tranter et al., 2002). Glacial runoff can contain elevated concentrations of key nutrients such as iron (Raiswell et al., 2006; Bhatia et al., 2013; Hawkings et al., 2014), phosphorus (Hawkings et al., 2016), and silica (Meire et al., 2016; Hawkings et al., 2017) and therefore has a direct impact on the adjacent fjord environment (Wehrmann et al., 2014; Hopwood et al., 2015) and potentially the wider ocean.

Understanding how glaciation alters chemical fluxes and the underlying chemical weathering reactions is important for understanding how weathering reactions changed during glacial-interglacial cycles (Vance et al., 2009; AMAP, 2017; Hawkings et al., 2017). If calcite and sulfide weathering dominate fluxes in glacial catchments, as concluded from studies of alpine glaciers, then these areas would not contribute to long-term removal of CO_2, and may even be a source (Sharp et al., 1995; Torres et al., 2017). However, recent studies of ice sheets, in particular from outlet glaciers of the Greenland Ice Sheet, indicate that silicate weathering is dominant (Graly et al., 2014; Hindshaw et al., 2014; Andrews and Jacobson, 2018) and therefore large-scale glaciation could contribute to the drawdown of atmospheric CO_2 over geological timescales (Walker et al., 1981; Berner et al., 1983).

A first estimate of the relative contributions of carbonate and silicate weathering to dissolved fluxes can be done by applying an end-member mixing analysis to major ion concentrations, utilizing "ideal" end-members (e.g., Gaillardet et al., 1999). However, this method is particularly problematic in glacierized catchments due to weathering incongruency (net effect of dissolution and precipitation/adsorprtion reactions both with respect to bulk rock and with respect to individual minerals), ion exchange and adsorption reactions which occur in glacial streams characterized by high sediment loads and dilute solute concentrations (e.g., Tranter, 2003). For example, the use of end-member ion ratios such as Ca/Na to calculate the relative proportions of carbonate and silicate weathering could overestimate the carbonate contribution if the preferential release of Ca from individual silicate minerals is not accounted for (Oliva et al., 2004; Hindshaw et al., 2011). Isotope tracers (stable and radiogenic) have been developed in recent decades to refine the apportioning of carbonate and silicate weathering in catchment studies (e.g., Blum et al., 1994; Bullen and Bailey, 2005; Nezat et al., 2010; Sullivan et al., 2016).

Magnesium (Mg) and lithium (Li) isotopes have shown promise at tracing weathering sources and processes (Tomascak et al., 2016; Teng, 2017) and have both been applied to study glacial weathering in the Kangerlussuaq area of West Greenland (**Figure 1**, Wimpenny et al., 2010, 2011). Magnesium is the 5th most abundant element in the continental crust (MgO = 3.7 wt.%, Wedepohl, 1995) and it is intimately coupled to the carbon cycle through the formation of magnesium carbonates (Berner et al., 1983). Carbonate δ^{26}Mg values (−6 to 0‰) tend to be lower than silicate rocks (−1 to +2‰) potentially enabling the partitioning of carbonate and silicate weathering (Teng, 2017). However, Mg isotopes are also fractionated during secondary clay formation and biological processes (Tomascak et al., 2016). Lithium is a trace element predominantly hosted in silicate rocks (Huh et al., 1998) and as a consequence, Li isotopes have the potential to be a tracer of silicate weathering (e.g., Misra and Froelich, 2012). In natural systems secondary mineral formation and/or adsorption onto particles imparts a large (often >10‰) fractionation and biological processes have minimal impact (e.g., Pistiner and Henderson, 2003; Vigier et al., 2008; Clergue et al., 2015). It is therefore hypothesized that the Li isotopic composition of rivers provides information on the balance between dissolution of primary (silicate) minerals and secondary mineral formation occurring in a catchment (e.g., Dellinger et al., 2015). Waters draining from the Greenland ice sheet were found to have lower δ^{26}Mg values compared to suspended sediment and this was attributed to disseminated carbonate weathering (Wimpenny et al., 2011). The δ^{7}Li values were higher than suspended sediment and the authors concluded this was due to adsorption to subglacially formed amorphous iron hydroxides (Wimpenny et al., 2010). Nevertheless, mineral separates to constrain local end-members were not analyzed, which leads to an element of uncertainty in source apportionment.

Research on the δ^{26}Mg values of mineral separates has demonstrated variation in δ^{26}Mg values which in some cases overlaps with the δ^{26}Mg range in carbonate rocks (−5.57 to −0.38‰, Teng, 2017), e.g., biotite (−0.40 to +0.44‰, Shen et al., 2009; Liu S.-A. et al., 2010; Ryu et al., 2011), chlorite (−1.82 to +0.40‰, Ryu et al., 2011; Pogge von Strandmann et al., 2015; Chapela Lara et al., 2017), clinopyroxene (−0.62 to +0.43‰, Pogge von Strandmann et al., 2011; Wang et al., 2012, 2014; Hu et al., 2016; Li et al., 2016; Chen et al., 2018; Stracke et al., 2018), and garnet (−1.96 to −0.37‰, Wang et al., 2012, 2014; Pogge von Strandmann et al., 2015; Hu et al., 2016; Li et al., 2016; Stracke et al., 2018). Within single rock samples, resolvable variation has also been observed e.g., 1.5‰ between chlorite and hornblende in granite (Ryu et al., 2011). This silicate mineral source variation in δ^{26}Mg has only recently begun to be acknowledged as a source of variation in river δ^{26}Mg values (Chapela Lara et al., 2017; Kimmig et al., 2018). Given that recent studies of chemical weathering in the Kangerlussuaq area of West Greenland have stressed the role of silicate weathering (Wimpenny et al., 2011; Andrews and Jacobson, 2018), we wanted to test whether silicate mineral variation in δ^{26}Mg values could also account for low δ^{26}Mg values in river samples from this area. There is less data on Li isotope variation between minerals (Teng et al., 2006; Pogge von Strandmann et al., 2011; Penniston-Dorland et al., 2017; Neukampf et al., 2019) but variation has been reported where there is a difference in coordination number (∼3‰, Wunder et al., 2007) and in field sites with a history of magmatic differentiation (−8 to +17‰, Marks et al., 2007). Dissolved δ^{7}Li values may therefore also be impacted by variations in silicate mineral isotopic compositions, particularly when the geology of the catchment is heterogeneous.

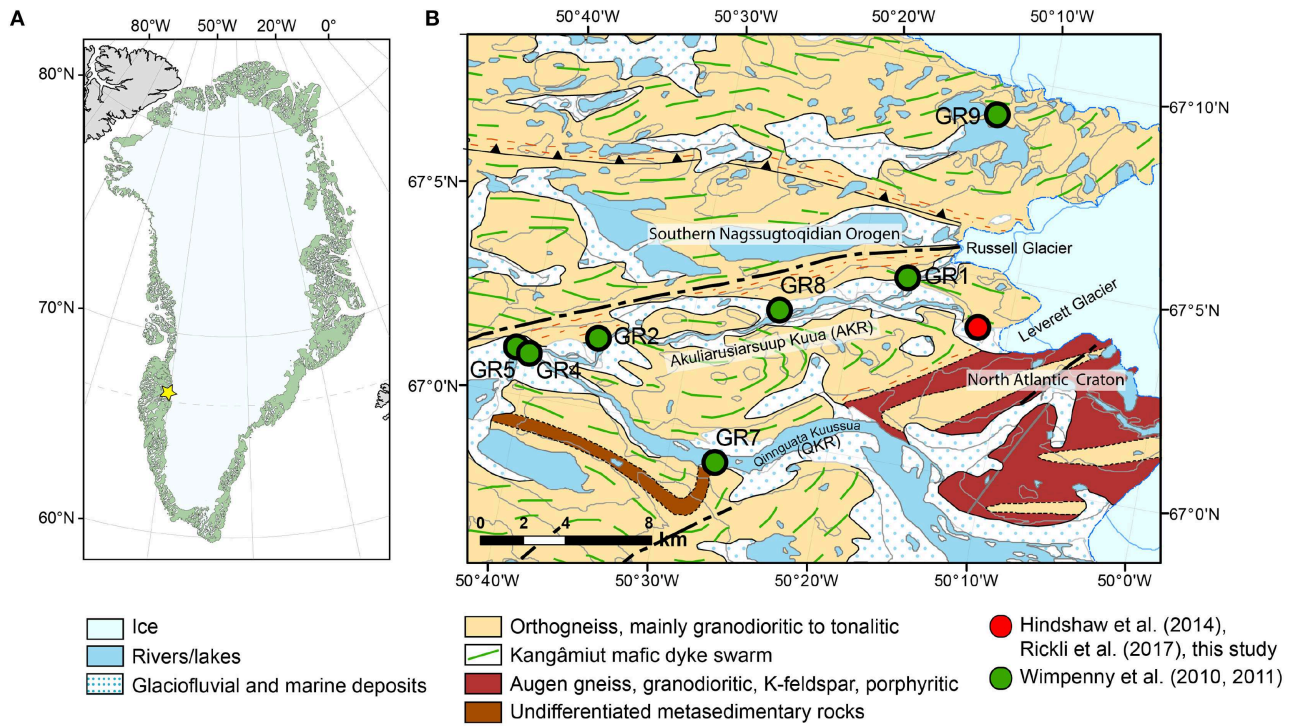

FIGURE 1 | (A) The study site is indicated by a yellow star. **(B)** Geological map of the Kangerlussuaq area of West Greenland. The location of the time series of water samples from the river draining Leverett Glacier analyzed in this study is marked as a red circle. River sediment and rock samples were also collected at this location. The water samples with a glacier contribution, bedload, suspended sediment, and bedrock samples analyzed by Wimpenny et al. (2010, 2011) are marked as green circles together with their sample names (GR1–GR9). Watson River refers to the river after the confluence of the Qinnguata Kuussua and Akuliarusiarsuup Kuua rivers. Geological basemap from Geological Survey of Denmark and Greenland, and Ministry of Mineral Resources under the Government of Greenland. Datum and projection: WGS84 UTM Zone 24N.

Previous work on water draining the Leverett Glacier, an outlet glacier in the Kangerlussuaq area (**Figure 1**), used Ca, Sr, Nd, and Hf data of water, rock, and mineral separates to constrain chemical weathering reactions contributing to the dissolved load (Hindshaw et al., 2014; Rickli et al., 2017). Our aim in this study was to analyse mineral separates, bulk rock samples, sediments, and water samples for δ^{26}Mg and δ^{7}Li in order to test whether the dissolution of silicate minerals previously identified as controlling the dissolved load composition in this catchment were consistent with dissolved δ^{26}Mg and δ^{7}Li values from this region or whether a carbonate contribution to dissolved δ^{26}Mg is indeed required.

2. FIELD SITE

Leverett Glacier is a land-terminating outlet glacier of the Greenland Ice Sheet situated on the west coast of Greenland ∼ 25 km east of Kangerlussuaq (Søndre Strømfjord, **Figure 1**). Together with Russell Glacier to the north these two glaciers form one of three subcatchments of the Watson River with a combined area of 900 km^2 (Lindbäck et al., 2015). Bartholomew et al. (2011) estimated the hydrological catchment of Leverett Glacier to be 600 km^2. The largest subcatchment (11,100 km^2) is the Ørkendalen subcatchment to the south containing the Qinnguata Kuussua River (QKR). The third subcatchment (Point 660) lies to the north of Russell Glacier and has an area of 40 km^2. Water draining Point 660 catchment feeds into water draining Russell Glacier. Approximately 19 km upstream from Kangerlussuaq this water merges with the Leverett River to form the Akuliarusiarsuup Kuua River (AKR). Unlike Leverett River, which has a single subglacial portal, the river draining past Russell Glacier has several inputs of water sourced from both non-glacial lakes and sub-glacial sources (Rennermalm et al., 2012). The watershed areas referred to above are the maximum summer extent as the catchment area grows and shrinks each melt-season in line with the expansion and contraction of the subglacial drainage network (Chandler et al., 2013). In addition, there is water piracy where the catchment areas and positions change with subglacial water pressure (Lindbäck et al., 2015). In 2009, the melt season was ∼115 days long at Leverett and a peak discharge of 317 m^3 s^{-1} was measured on 16th July (Bartholomew et al., 2011).

Leverett Glacier drains distinct tectonic units of Precambrian age (**Figure 1**). To the north of Leverett is the Southern Nagssugtoqidian Orogen, which is composed of re-worked epidote amphibolite to amphibolite facies basement tonalitic to granodioritic orthogneiss (Escher, 1971; Van Gool et al., 2002).

The orthogneisses were intruded by the 2.04 Ga Kangâmiut mafic dyke swarm (Cadman et al., 2001), now forming amphibolite lenses, with deformation increasing toward the north (Van Gool et al., 2002; Engström and Klint, 2014). To the south of Leverett is the North Atlantic Craton, composed of granulite-facies granodioritic augen orthogneiss and paragneiss locally (Escher et al., 1976; Henriksen et al., 2000). The augen orthogneiss was intruded by late Archaean felsic intrusions (45 km south of the Leverett Glacier) related to the Qôrqut granite (ca. 2.5 Ga, Escher et al., 1976; Nutman et al., 2010). See Brown et al. (1981) for a petrographic description of the Qôrqut granite. The exact boundary between the above-described tectonic units underneath the Greenland ice sheet is unknown.

The area experiences an Arctic climate with a mean annual temperature (2001–2011) of −3.9°C (Hanna et al., 2012). There are strong seasonal variations in temperature: the mean temperatures in winter and summer are −16.1 and +10.3°C, respectively (Hanna et al., 2012). The region receives relatively little precipitation [258 ± 63 mm (2001–2012), (Mernild et al., 2015)] and annual evapotranspiration exceeds annual precipitation (Johansson et al., 2015). In the non-glacierized area, permafrost is continuous with an active layer thickness of 0.1–2.5 m (Van Tatenhove, 1996).

3. METHODS

3.1. Water Samples

The Leverett River was sampled twice a day from 5 July to 1 August 2009 at 67°03.755′N, 50°11.874′W. The sampling location was ∼1 km downstream from the glacier front (**Figure 1**). At this location there was no braiding in the river channel and the water was turbulent. Therefore, we assume that the river was well-mixed and samples taken at the edge of the river are representative of bulk river water chemistry. Temperature and pH were measured *in situ* (Hanna HI 98160 pH meter). Water samples were collected in a bucket previously rinsed with river water and filtered on the day of collection through 0.2 μm nylon filters using a Nalgene filtration unit connected to a hand pump. Filtered samples were stored in pre-cleaned HDPE bottles and acidified to pH 2 with single-distilled concentrated HNO_3. Discharge was measured as described in Bartholomew et al. (2011). In terms of the number of days, the sampling campaign covered 24% of the 2009 melt-season and in terms of water flux it covered 45% of the total of that year.

The hydrology and chemistry of the Leverett River during the 2009 melt-season have previously been reported (Bartholomew et al., 2011; Hindshaw et al., 2014; Rickli et al., 2017) and the main results are summarized here. The hydrology was typical for a glacierized catchment with strong seasonal variation. Before June discharge was <6 m^3/s and rapidly increased to a maximum of 317 m^3/s on 16 July before decreasing again (Bartholomew et al., 2011). The sampling season was divided into three periods based on changes in hydrochemistry (Hindshaw et al., 2014). Immediately prior to the sampling period there was a spike in discharge linked to the sudden drainage of supraglacial lakes (**Figure 2**, Bartholomew et al., 2011). This pulse of water coincided with high pH, suspended sediment and ion concentrations. The first period (P1) was defined as the period from the start of measurements to the end of the marked decrease in element (**Figure 2**) and suspended sediment concentrations. The second period (P2) was characterized by increasing discharge and decreasing $^{87}Sr/^{86}Sr$ values. During this period the subglacial drainage system was expanding. The third period (P3) was characterized by decreasing discharge with a diurnal cycle. During P2 and P3 element concentrations were relatively stable (**Figure 2**). High radiogenic Sr and Ca isotope ratios at the start of the sampling period were interpreted to reflect flushed out water stored over winter with ions derived from chlorite and feldspar weathering. As the melt-season progressed and the subglacial drainage system expanded, the relative contribution of unradiogenic trace minerals such as epidote was inferred to increase as water-rock residence time decreased, resulting in the observed decrease in radiogenic Sr and Ca isotope ratios (Hindshaw et al., 2014). For this study a subset of ten samples were selected for isotope analyses covering all three hydrological periods (**Figure 2**). Samples were selected to coincide with those already measured for Ca and Sr isotopes. We focussed in particular on P2 where the subglacial drainage system expands and where a decrease in $^{87}Sr/^{86}Sr$ from 0.745 to 0.741 was interpreted to represent a change in the relative contribution of different mineral weathering reactions to the dissolved load (Hindshaw et al., 2014).

Wimpenny et al. (2010, 2011) collected their glacial samples between 11 and 14 July 2006 but discharge data was not reported. Discharge data from the Watson River at Kangerlussuaq shows that during this period discharge was increasing and comparable to the form of the hydrograph in 2009 for the same time period (van As et al., 2017). Both years had similar total water flux: 5.4 ± 2.9 km^3 in 2006 and 4.9 ± 0.9 km^3 in 2009, and peak flux: 1,690 ± 1,190 m^3 s^{-1} in 2006 and 1,430 ± 210 m^3 s^{-1} in 2009 (van As et al., 2017). Therefore, these samples were likely collected when discharge conditions resembled those of P2 and we can assume that the hydrological conditions during the two studies are comparable.

3.2. Rock, Sediment, and Mineral Separates

Four rock samples representing the dominant rocks types on the north side of Leverett Glacier (Southern Nagssugtoqidian Orogen, **Figure 1**) were collected and described in Hindshaw et al. (2014) and Rickli et al. (2017). These rock samples were two orthogneisses and two amphibolites and were located within 1 km of where the water samples were taken. In addition, two bulk samples of river sediment were analyzed. These samples were analyzed in this study for Mg and Li isotopes.

A sample of augen gneiss from the North Atlantic Craton (**Figure 1**) collected 20 km southwest of Leverett (50.338066 W, 66.894928 N) by the Geological Survey of Denmark and Greenland (GEUS) was analyzed in Rickli et al. (2017) where this sample was referred to as "Archaean granite." Rickli et al. (2017) concluded, based on Nd isotope data, that the contribution of gneiss from the North Atlantic Craton to the dissolved load of Leverett River was negligible and therefore this rock was

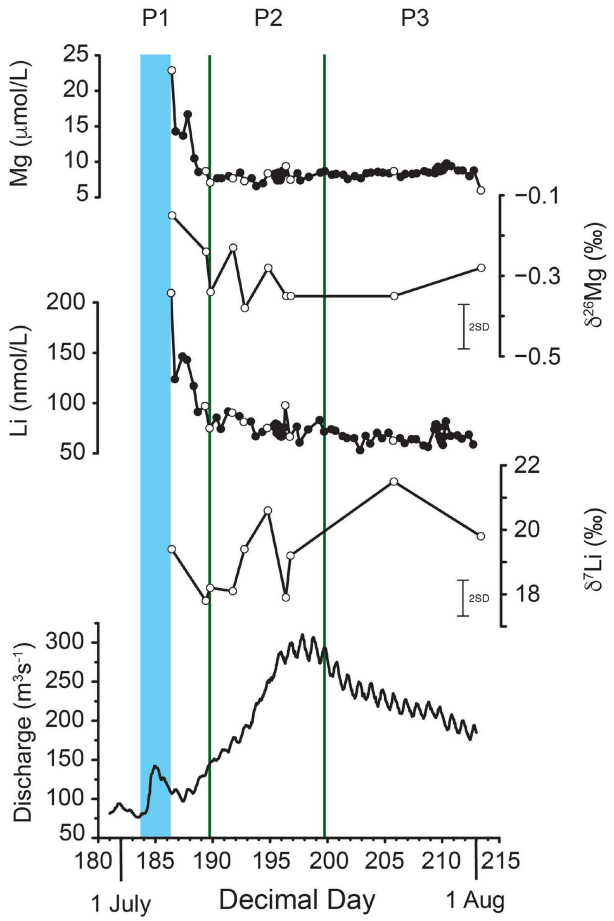

FIGURE 2 | Time series. From top to bottom: Mg concentration, δ^{26}Mg, Li concentration, δ^{7}Li and discharge. White circles are samples analyzed for this study and black circles are time series data from Hindshaw et al. (2014). The blue band marks the fourth outburst event of 2009 which coincided with the drainage of a supraglacial lake (Bartholomew et al., 2011). The green lines mark indicate divisions between three hydrological periods (P1, P2, and P3) identified by Hindshaw et al. (2014) based on changes in hydrochemistry. P1 is influenced by the outburst event, P2 is the rising limb of the hydrograph, and P3 the falling limb.

not analyzed for Li and Mg isotopes (see further discussion in section 5.3).

Rock samples were washed, weathered surfaces removed with a diamond saw and crushed using a jaw crusher. A portion of each rock sample and all of the other solid samples were ground to a fine powder using a rotary disc mill with an agate grinding set for further analysis. The remainder of the rock samples were ground to <1,000 μm and mineral separates were obtained from the <425 μm fraction using heavy liquids, magnetic separation and hand-picking.

Two river sediments (Sed1 and Sed2, **Table 1**) were collected from the riverbank, and can therefore be considered comparable to the bedload samples reported in Wimpenny et al. (2010, 2011).

Mineral abundances were obtained by point counting on thin section (rock samples) and EPOXY mounts (sediments) microphotographs combined with scanning electron microscope (SEM) back-scattered images (Hitachi S-3500N microscope equipped with Thermo Noran energy dispersive spectrometer at the University of Bristol) and element maps.

The primary rock forming minerals in the orthogneiss samples (Ro2 and Ro4) are K-feldspar (24–43 wt.%), plagioclase (21–49 wt.%), and quartz (22–27 wt.%). These rocks also contain chlorite (2–7 wt.%) and minor (<3 wt.%) epidote, titanite, zircon, hornblende, and apatite (Rickli et al., 2017). In both orthogneisses, chlorite and epidote replaced biotite during green schist metamorphism. The garnet amphibolite rock sample Ro1 is primarily composed of hornblende (71 wt.%), plagioclase (11 wt.%), and quartz (8 wt.%) together with lesser amounts of garnet (5 wt.%), titanite (3 wt.%), and magnetite (2 wt.%) (Rickli et al., 2017). Amphibolite Ro3 contains hornblende (47 wt.%), clinopyroxene (24 wt.%), plagioclase (15 wt.%), and scapolite (10 wt.%) and trace minerals are epidote (3 wt.%) and titanite (<1 wt.%) (Rickli et al., 2017). Although the alteration of plagioclase to Ca-rich carbonate was observed in the orthogneiss samples (Ro2 and Ro4, Hindshaw et al., 2014) through saussuritization, the presence of Mg-bearing carbonate minerals was not detected in SEM chemical maps of the Leverett catchment rocks and sediments. For this study minerals with high Mg concentration were selected for analysis: garnet, hornblende, clinopyroxene, and chlorite.

The mineralogy of sediment samples reflected a mixture of gneiss and amphibolite and contained plagioclase (39–44%), quartz (33–37%), K-feldspar (7–16%), hornblende (7–11%), garnet (2–4%), clinopyroxene (<3%), and minor (<2%) apatite, biotite, chlorite, epidote, ilmenite, orthopyroxene, magnetite, titanite, and zircon (Rickli et al., 2017).

Approximately 0.2 g of each rock powder or sediment sample and 0.02 g of each mineral were digested in a mixture of concentrated, single-distilled HNO_3, HCl, and HF. The solution was repeatedly dried down and redissolved until clear and was finally redissolved in 2% HNO_3 for cation analysis.

3.3. Concentration Analysis

Magnesium concentrations in water, rock, and mineral separate samples were measured by inductively-coupled plasma optical emission spectrometry (ICP-OES, Vista-MPX, Varian Inc., USA at ETH Zurich) as described and reported in Hindshaw et al. (2014). The Mg concentration of the water standard SLRS-4 (National Research Council Canada) was 1,686 ± 40 μg L^{-1} (2SD, $n = 7$) compared to a recommended value of 1,600 μg L^{-1} (Yeghicheyan et al., 2007). Magnesium concentrations of minerals in rocks were additionally determined using a Cameca SX100 electron microprobe analyser (EMPA) at University of Bristol and a JEOL JXA-8200 EPMA at ETH Zurich, with a 15 kV accelerating voltage and a beam current of 20 nA. Natural and synthetic silicates and oxides were used as standards and the error on concentration measurements was typically less than 2%. Lithium concentrations were measured by ICP-OES. The Li concentration of the water standard SLRS-4 (National Research Council Canada) was 0.56 ± 0.03 μg L^{-1} (2SD, $n = 6$) compared to a recommended value of 0.54 μg L^{-1} (Yeghicheyan et al., 2007).

TABLE 1 | Magnesium and lithium concentrations and isotope ratios of rocks, mineral separates, and river sediment samples.

Name	Abundance wt.%	Mg[a] g/kg	Mg[b] g/kg	Fraction[c] Mg	δ^{25}Mg ‰	2SD	δ^{26}Mg ‰	2SD	Li mg/kg	Fraction[d] Li	δ^{7}Li ‰	2SD
Ro1 - Garnet Amphibolite		48.5			–0.10	0.05	–0.20	0.06	5.2		6.8	0.7
Garnet	5	11.2	10.9	0.02	–0.84	0.04	–1.63	0.06	5.3	0.01	6.6	1.3
Hornblende	71	41.9	46.2	0.98	–0.08	0.10	–0.16	0.11	46.4	0.96	6.9	0.4
Ro3 - Amphibolite		47.0			0.04	0.08	0.09	0.13	9.19		8.3	0.1
Clinopyroxene	24	70.0	70.3	0.37	–0.07	0.03	–0.14	0.11	44.3	0.43	6.5	0.3
Hornblende	47	62.4	59.1	0.63	0.03	0.04	0.06	0.08	26.4	0.50	12.1	0.2
Ro2 - Orthogneiss		6.5			–0.04	0.06	–0.08	0.09	5.4		6.3	0.9
Chlorite	2	76.3	72.7	0.86	–0.11	0.05	–0.21	0.11	59.2	0.36	3.4	0.2
K-feldspar	24	0.9	0.0	0.11	n.m.	n.m.	n.m.	n.m.	10.0	0.64	n.m.	n.m.
Plagioclase	49	0.1	0.3	0.03	n.m.	n.m.	n.m.	n.m.	0.0	0.00	n.m.	n.m.
Ro4 - Orthogneiss		10.8			–0.09	0.02	–0.20	0.02	6.3		5.0	0.8
Chlorite	7	32.5	82.7	0.96	–0.15	0.02	–0.29	0.05	117.9	0.66	3.2	2.0
Hornblende	<1	38.1	n.m.	0.00	–0.15	0.05	–0.28	0.08	n.m.	0.00	n.m.	n.m.
Epidote	3	1.5	0.6	0.02	n.m.	n.m.	n.m.	n.m.	12	0.03	n.m.	n.m.
Feldspar[e]	64	0.1	0.1	0.03	n.m.	n.m.	n.m.	n.m.	6	0.31	n.m.	n.m.
Feldspar+Epidote[f]	67	*0.7*		0.04					*6.4*	0.34	*8.5*	*2.1*
Other solid samples												
Sed1		20.9			–0.18	0.14	–0.33	0.16	n.m.		4.9	0.4
Sed2		12.4			–0.26	0.07	–0.48	0.15	81.2		n.m.	n.m.

*Rock samples are all from the Southern Nagssugtoqidian Orogen (**Figure 1**). Mineral abundances and Mg concentrations are from Hindshaw et al. (2014).*
n.m., not measured.
[a] *Measured by ICP-OES.*
[b] *Measured by microprobe.*
[c] *Calculated using ICP-OES concentrations.*
[d] *Plagioclase and epidote account for the rest of the Li fraction in Ro1 and Ro3.*
[e] *Feldspar = Plagioclase and K-feldspar.*
[f] *Values in italics are calculated by mass balance using the fraction and concentrations of Mg and Li reported for the respective minerals.*

3.4. Isotope Analysis

An aliquot of each sample, corresponding to ∼ 15 ng Li was dried down in a teflon beaker. The solid residue was re-dissolved in concentrated HNO_3, dried down again and re-dissolved in 0.4 M HCl for column chemistry. The first column contained 1 mL Bio-Rad AG 50W-X12 200-400 mesh resin. In the first column the sample was eluted in 0.4 M HCl and the first 15 of 50 mL containing Li and Na were collected. The Mg cut was then collected in 15 mL 1 M HCl. For rocks and mineral samples, a 0.5 M HF step was inserted prior to the 0.4 M HCl elution step in order to elute Al, Ti, and Zr (Tipper et al., 2008). The Mg cut from the first column pass was passed through the column a second time and Mg was collected in a small volume of 6 M HCl in order to minimize procedural blanks (Tipper et al., 2008). Lithium was purified from the Li-Na cut using a column containing 3 mL Bio-Rad AG 50W-X12 200–400 mesh resin, eluting with 0.2 M HCl (James and Palmer, 2000; Hindshaw et al., 2018). Standards were processed in an identical manner to samples.

Both isotope systems were measured on a Neptune Plus MC-ICP-MS (Thermo, University of Cambridge) using an APEX sample introduction system. Magnesium isotopes were run at 100 ppb and Li at 5 ppb. Magnesium and Li were standard-sample bracketed to DSM3 and L-SVEC (NIST RM 8545), respectively. For each isotope system mono-elemental secondary standards were analyzed: ^{6}Li-N and ^{7}Li-N for Li, and "Cambridge1" and "Zurich1" for Mg. The values obtained for these standards are reported in **Table 2** and are in agreement with previously reported values (Tipper et al., 2006, 2012b; Carignan et al., 2007; Millot et al., 2010; Wimpenny et al., 2014). Seawater (OSIL IAPSO batch P157) was processed identically to the water samples and gave values of δ^{26}Mg = –0.81 ± 0.11 (2SD, n = 5) and δ^{7}Li = +31.4 ± 0.4 (2SD, n = 3), in agreement with both our long-term values for this standard (δ^{26}Mg = –0.80 ± 0.11, 2SD, n = 25; δ^{7}Li = +30.8 ± 1.1, 2SD, n = 45) and literature values (δ^{26}Mg = –0.83‰, Teng et al., 2015; δ^{7}Li = +30.8‰, Rosner et al., 2007). The synthetic water standard CCS2 (Tipper et al., 2008) and USGS granite G-2 were measured for Mg isotopes giving values of −2.70 ± 0.14 (2SD, n = 13) and −0.05 ± 0.13 (2SD, n = 5) compared to the respective literature values of −2.71 ± 0.07‰ (Tipper et al., 2008) and −0.15 ± 0.07‰ (Teng et al., 2015). Lithium isotope measurements of USGS granite G-2 were +0.9 ± 1.0‰ (2SD, n = 6) compared to literature values of +0.1 ± 1.8‰ (Barnes et al., 2012), +0.1 ± 0.8‰ (Phan et al., 2016), and +0.3 ± 1.9‰ (Liu X.-M. et al., 2010). The long-term 2SD values from measurements of seawater standards (δ^{7}Li = ±1.1‰, δ^{26}Mg = ±0.11‰) are used as a measure of the overall uncertainty of the analytical procedure and is indicated on all figures.

TABLE 2 | Major cation (Hindshaw et al., 2014) and isotopic composition of Leverett River water samples in 2009.

Sample name	Local time	Runoff (m/s)	pH	Ca μmol/L	Mg μmol/L	Na μmol/L	K μmol/L	Li nmol/L	δ^7Li ‰	2SD	δ^{25}Mg ‰	2SD	δ^{26}Mg ‰	2SD
0705a.m.	09:10	108	9.32	67.7	22.9	110.1	58.4	192.5	19.4	0.9	–0.07	0.04	-0.15	0.09
0708a.m.	08:25	130	8.48	34.0	8.7	48.4	32.1	98.4	17.8	0.2	–0.12	0.07	–0.24	0.12
0708p.m.	17:45	145	8.02	26.6	7.1	35.9	25.2	78.1	18.2	0.2	–0.18	0.04	–0.34	0.07
0710p.m.	17:00	175	7.68	30.0	7.7	38.9	39.4	87.4	18.1	0.4	–0.12	0.04	–0.23	0.09
0711p.m.	17:15	191	8.28	28.6	7.3	36.4	25.3	83.0	19.4	0.1	–0.19	0.02	–0.38	0.06
0713p.m.	18:20	249	8.07	28.4	8.4	32.9	27.3	78.3	20.6	0.3	–0.14	0.00	–0.28	0.06
0715a.m.	08:00	274	8.25	38.8	9.4	39.4	28.4	109.7	17.9	0.3	–0.19	0.13	–0.35	0.16
0715p.m.	17:35	299	7.96	29.2	7.5	33.3	22.0	87.3	19.2	0.4	–0.18	0.10	–0.35	0.15
0724p.m.	17:50	235	7.88	33.5	8.7	36.7	23.9	77.9	21.5	0.3	–0.18	0.01	–0.35	0.02
0801a.m.	08:00	172	7.88	20.8	6.0	35.0	21.5		19.8	0.1	–0.14	0.01	–0.28	0.00
Mono-elemental standards														
^{6}Li-N ($n = 59$)									–8.1	0.9				
^{7}Li-N ($n = 50$)									30.2	0.9				
Cambridge1 ($n = 29$)											–1.35	0.06	–2.61	0.12
Zurich1 ($n = 21$)											–1.73	0.10	–3.35	0.20

4. RESULTS

4.1. Rock and Mineral Separates

The range in isotope values of the four bulk rock samples is δ^{26}Mg = –0.20 to +0.09‰ and δ^7Li = +5.0 to +8.3‰ (**Table 1**). The isotopic compositions of the amphibolite samples (Ro1 and Ro3) overlap with those of the orthogneiss samples (Ro2 and Ro4) for δ^7Li and δ^{26}Mg. For Li, the range in bulk rock δ^7Li values agrees with the range measured by Wimpenny et al. (2010) for rocks from the Southern Nagssugtoqidian Orogen in the Kangerlussuaq region (+5.8 to +10.4‰, **Figure 1**, **3**).

The river sediment sample Sed1 has a δ^7Li value of +4.9‰ (**Table 1**) which is at the lower end of the range measured in bulk rock samples from this study and bedload samples (+4.8 to +6.9‰) measured by Wimpenny et al. (2010) (**Figure 3**). For Mg, the δ^{26}Mg values of the river sediment samples (–0.33 and –0.48‰, **Table 1**) are in the same range as bedload samples reported in Wimpenny et al. (2011) (–0.43 to –0.53‰), but are lower than the rock samples from this study (**Figure 3**). Based on the major element composition and plagioclase chemistry of the river sediment samples, it was determined that of the two observed orthogneiss varieties (pink and gray), gray orthogneisses like Ro4 have a dominant contribution to the sediment load (Hindshaw et al., 2014). This conclusion is supported by the fact that for both Li and Mg, rock Ro4 is closest in isotope composition to the river sediment (**Figure 3**). The lower δ^{26}Mg value of the river sediment samples compared to Ro4 is likely due to the contribution of garnet (2–4%, Rickli et al., 2017) which is not present in Ro4 and is derived from the amphibolite rocks.

The measured Mg concentrations in the minerals obtained by ICP-OES agree well with the analysis of those same minerals by microprobe (**Table 1**). Two exceptions are K-feldspar in Ro2, where the Mg concentration obtained by ICP-OES is over ten times greater than the microprobe measurement and chlorite in Ro4, where the Mg concentration obtained by ICP-OES is half the microprobe measurement. We note that the isotope and concentration values reported by ICP-OES are unlikely to reflect the pure mineral phase as they will also include a contribution from inclusions and/or trace amounts of other minerals not removed during hand-picking. Both discrepancies are likely caused by the alteration of K-feldspar to chlorite (Garrels and Howard, 1957) making it difficult to separate these minerals during hand-picking. Based on a mass balance calculation, nearly all the Mg and Li in Ro1 is contained in hornblende (>96%) whereas in Ro3 both clinopyroxene and hornblende host these elements (**Table 1**). In the orthogneiss samples the largest fraction of Mg and Li in Ro4 is in chlorite (96 and 66%, respectively) and chlorite is also the primary host of Mg in Ro2 (86%). Lithium in Ro2 is mainly contained in K-feldspar (including any potential inclusions) (64%, **Table 1**) and the remaining Li is in chlorite (36%, **Table 1**).

The mineral separates display a large range in δ^{26}Mg from –1.63‰ in garnet (Ro1) to +0.06‰ in hornblende (Ro3, **Table 1**). The range in δ^{26}Mg is comparable to that found within mineral separates from a granodiorite from Boulder Creek, USA (1.53‰, Ryu et al., 2011). Taking all the mineral separates together, hornblende has higher δ^{26}Mg values compared to chlorite (**Figure 3**), consistent with mineral separate data reported by Ryu et al. (2011) but in contrast to Chapela Lara et al. (2017) who observed that chlorite had higher δ^{26}Mg values than both pyroxene (by ∼0.2‰) and amphibole (by ∼0.5‰), though they note that the amphiboles were heavily altered. Garnet had lower δ^{26}Mg values compared to clinopyroxene (**Figure 3**), consistent with previous studies (Wang et al., 2012, 2014; Hu et al., 2016; Li et al., 2016). A large inter-mineral range is also observed in δ^7Li values from +3.2‰ in chlorite (Ro4) to +12.1‰ in hornblende (Ro3, **Table 1**). As for Mg isotopes, hornblende mineral separates have higher δ^7Li values compared to chlorite mineral separates (**Figure 3**), in agreement with Marks et al. (2007).

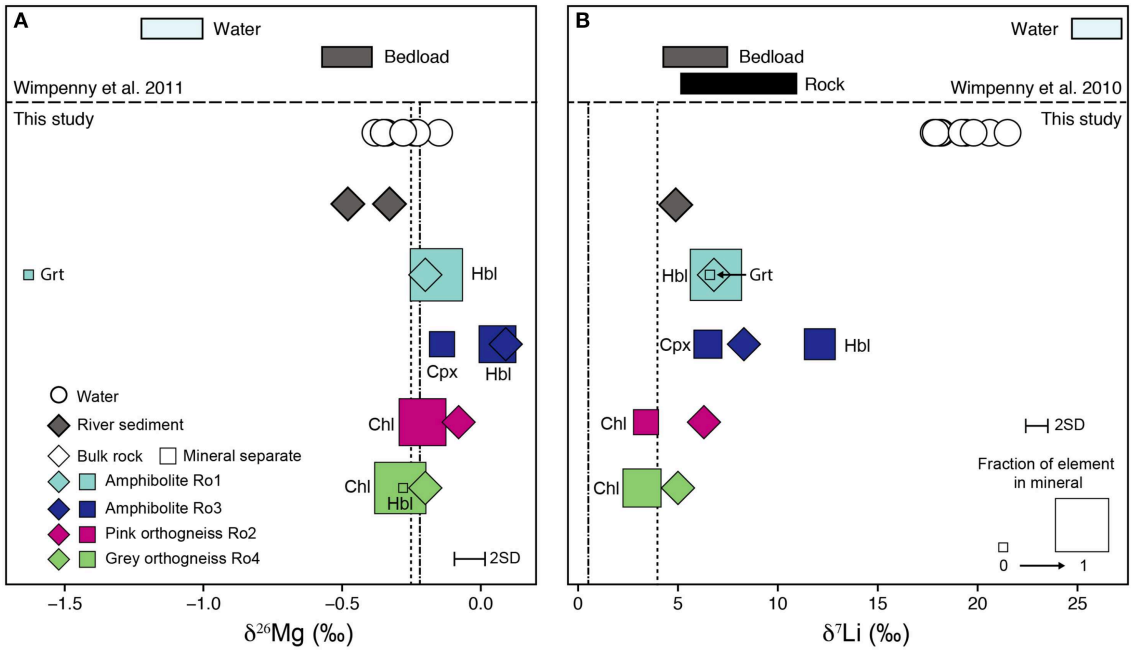

FIGURE 3 | Range of magnesium **(A)** and lithium **(B)** isotope values measured in the rocks, mineral separates, and river water of the Leverett Glacier catchment. Mineral abbreviations are: Grt, garnet; Hbl, hornblende; Chl, chlorite; Cpx, clinopyroxene. The fraction of the element contained in each mineral (**Table 1**) is indicated by the size of the square. Also shown are data from Wimpenny et al. (2010, 2011) which were collected in the same region, but not the same outlet glacier (**Figure 1**). The vertical dotted lines depict the normal mantle value for Mg (–0.25‰, Teng et al., 2010) and the upper mantle value for Li (+4‰, Teng et al., 2004). The dash-dot lines indicate average upper continental crust values for Mg (–0.22‰, Li et al., 2010) and Li (+0.6‰, Sauzéat et al., 2015).

4.2. Hydrochemistry

Similar to Ca and Sr concentrations, Mg and Li concentrations are highest at the start of the sampling period (Mg 0.6 mg/L and Li 1.3 μg/L) and rapidly decrease over a period of 4 days (**Figure 2**, Hindshaw et al., 2014). After the initial decrease, concentrations are stable (Mg ∼0.2 mg/L and Li ∼0.6 μg/L) with a diurnal cycle (**Table 2**). The stable isotope values of the water samples range from δ^{26}Mg = –0.15 to –0.38‰ and δ^{7}Li = +17.8 to +21.5‰ and no obvious temporal trend is observed in either Li or Mg isotope values despite the aforementioned changes in concentrations and subglacial drainage conditions (**Figure 2**, **Table 2**). Despite the proximity of Leverett Glacier to the sampling locations in Wimpenny et al. (2010, 2011) (**Figure 1**), the Li and Mg isotope values for the water samples in this study are distinct, having lower δ^{7}Li and higher δ^{26}Mg values (**Figure 3**).

5. DISCUSSION

5.1. Inter-mineral Isotope Variation

The range in δ^{26}Mg and δ^{7}Li between all the mineral separates measured in the four rock samples is 1.69 and 8.8‰ respectively. Inter-mineral variations in isotope values have been attributed to equilibrium fractionation (Schauble, 2004, 2011; Wunder et al., 2007; Liu et al., 2018). Coordination number is the first order control: heavy isotopes are preferentially incorporated into sites with a low coordination number (CN) (Oi et al., 1989). Excluding garnet (see later), there is a statistically significant correlation between the δ^{26}Mg and δ^{7}Li values of the measured minerals and bulk rock samples (R^2 = 0.67, p < 0.01, **Figure 4**). This trend is consistent with the similar chemical radii of the two elements such that Li can readily substitute for Mg and both elements will therefore likely experience similar bonding environments in a given mineral.

Based on equilibrium fractionation models at a range of temperatures relevant to weathering and igneous processes (273–2,000 K), the δ^{26}Mg and δ^{7}Li values of garnet (CN = 8) are predicted to be lower (Schauble, 2011; Huang et al., 2013) compared to hornblende (CN = 6/5, Wunder et al., 2007) and for Mg isotopes this is what we observe (**Figure 3**). In contrast, the δ^{7}Li value of garnet is not markedly lower than the other minerals as would be predicted if Li was in the dodecahedral site (e.g., Yang et al., 2009). Studies of lithium-rich synthetic garnets have demonstrated that Li can be contained in sites with CNs of 4 and 6 (Mazza, 1988; O'Callaghan et al., 2008; Cussen, 2010; Rettenwander et al., 2016). If this were true for natural garnets then the Li CN may be less than 8 accounting for the δ^{7}Li value that is indistinguishable from the hornblende separate in the same rock (Ro1, **Figure 4**). The low δ^{26}Mg value of garnet, 1.34‰ lower than the δ^{26}Mg values for the other minerals (**Figure 3**), is consistent with data from clinopyroxene-garnet pairs where garnet always has lower δ^{26}Mg values compared to clinopyroxene (Huang et al., 2013; Stracke et al., 2018). The magnitude of the difference increases as metamorphism temperature decreases (Huang et al., 2013; Stracke et al., 2018). Therefore, the relatively large difference between garnet and clinopyroxene observed in

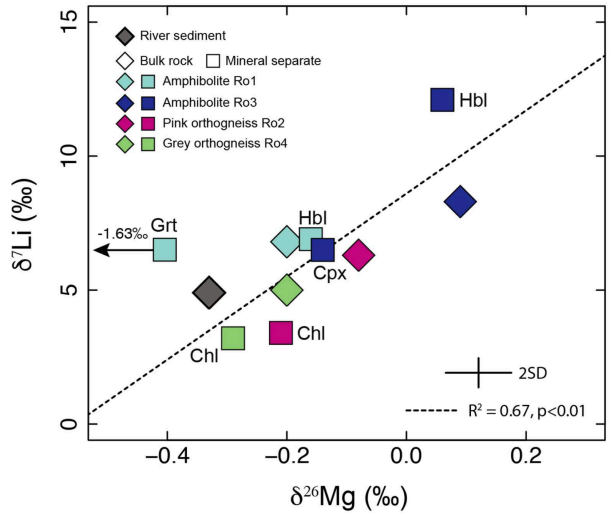

FIGURE 4 | Excluding garnet, where Li and Mg may be held in sites with different coordination numbers, a positive relationship is observed between the δ^{26}Mg and δ^{7}Li values of the rocks (diamonds) and mineral separates (squares). Mineral abbreviations are: Grt, garnet; Hbl, hornblende; Chl, chlorite; Cpx, clinopyroxene.

this study is consistent with the relatively low temperatures of amphibolite facies metamorphism experienced by rocks of the Southern Nagssugtoqidian Orogen (Henriksen et al., 2000).

5.2. Assessment of External Inputs to the Dissolved Load

As the river emanates directly from the mouth of the glacier we consider vegetation (which in the wider field setting is sparse) to have negligible impact on biogeochemical processes at this field site and no vegetation samples were analyzed. In addition to water derived from subglacial weathering reactions, solutes could be derived from surficial inputs such as dust deposition and meteorological precipitation. It neither rained nor snowed during the duration of the sampling campaign. However, information on atmospheric deposition could be gained from supraglacial streams which are assumed to be the water source most likely to be influenced by atmospheric deposition (melting snow/ice and dust). Five supraglacial streams were sampled in Hindshaw et al. (2014) and were combined for analysis. The Mg concentration was <0.05 μmol L^{-1} and the Li concentration was below the detection limit. The low concentration of Li and Mg in supraglacial streams implies that precipitation and dust are unlikely to affect subglacial river concentrations and isotope ratios. The effect of meteorological precipitation on Mg and Li isotope ratios can further be assessed by assuming that all Cl in the river is derived from seawater and correcting the isotope ratios according to the following equation:

$$\delta X^{*} = \frac{\delta X_r \cdot X_r - ((X/Cl)_{sw} \cdot Cl_r) \cdot \delta X_{sw}}{X_r - (X/Cl)_{sw} \cdot Cl_r} \quad (1)$$

where subscripts *r* and *sw* stand for "river" and "seawater," respectively and X is either Mg or Li. The corrected ratios are within experimental uncertainty of the uncorrected ratios (<0.04‰ and <0.05‰ difference for δ^{26}Mg and δ^{7}Li, respectively). The negligible impact of meteorological precipitation is in agreement with Ca and Sr isotope data for this region (Hindshaw et al., 2014; Andrews and Jacobson, 2018). We therefore assume that the dominant solute source to the river is subglacial weathering reactions and as a result data was not corrected for additional precipitation inputs, consistent with Wimpenny et al. (2010, 2011).

5.3. Mineral Source Control on River Water Isotope Ratios

The Mg and Li stable isotope ratios of the dissolved load can reflect mixing between distinct solute sources and/or fractionation processes. We will examine each of these in turn.

Mixing between Mg derived from isotopically distinct silicate mineral sources has been observed in a variety of catchments (Chapela Lara et al., 2017; Kimmig et al., 2018). For Mg, the δ^{26}Mg isotope ratios of the Leverett River water samples are intermediate between the garnet (–1.63‰) and hornblende (+0.06‰). The δ^{26}Mg values measured in the river could therefore reflect mixing between different mineral sources. Previous work utilizing Ca and Sr isotope ratios concluded that for these elements, the primary mineral sources contributing to the dissolved load were minerals from orthogneiss Ro4: feldspar, chlorite, and epidote (Hindshaw et al., 2014). In addition, the weathering of garnet, titanite, hornblende, and apatite from Ro4 and other rocks was invoked to explain the radiogenic Hf and Nd isotope compositions in river water (Rickli et al., 2017).

In orthogneiss Ro4, Mg is primarily hosted in chlorite and the δ^{26}Mg value of this mineral separate (–0.29‰) is identical within error of the average river water (–0.30 ± 0.14‰, 2SD). However, the weathering of chlorite only is inconsistent with the $^{87}Sr/^{86}Sr$ river water data which indicate mixing with unradiogenic feldspar and epidote (Hindshaw et al., 2014). We have not measured the δ^{26}Mg values of feldspar and epidote from Ro4. We can estimate the δ^{26}Mg value of a combined feldspar-epidote fraction based on mass balance, but since the bulk rock δ^{26}Mg value (–0.20 ± 0.11‰) is within analytical uncertainty of the chlorite separate (–0.29 ± 0.11‰, **Table 1**), this calculation is poorly constrained. However, based on the observation that inter-mineral variation between minerals is minor when Mg is octahedrally coordinated (∼0.06‰, Liu S.-A. et al., 2010), we infer that the Mg isotope composition of a combined epidote-feldspar fraction is close to that of chlorite and we assume the bulk rock value of –0.20‰ for this fraction. A mixing line in δ^{26}Mg vs. $^{87}Sr/^{86}Sr$ space between chlorite and "feldspar-epidote" passes through the river water sample points (**Figure 5**). Therefore, similar to radiogenic Sr and Ca (Hindshaw et al., 2014), the dissolved δ^{26}Mg values would be consistent with the dissolution of this group of minerals. However, we emphasize that the fraction of Mg hosted in plagioclase and epidote is low (4%, **Table 1**), and therefore these two minerals are expected to have a minor contribution to dissolved Mg.

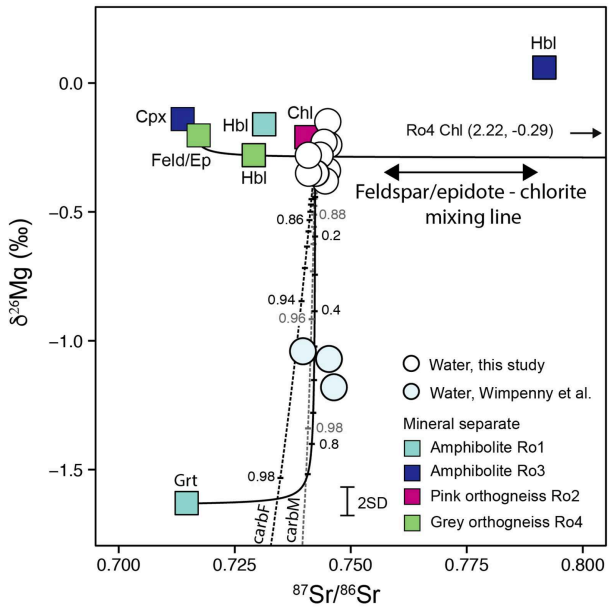

FIGURE 5 | δ^{26}Mg vs. $^{87}Sr/^{86}Sr$. Previous work demonstrated the dominance of orthogneiss Ro4, in particular chlorite, feldspar, and epidote, to the dissolved and sediment load of the Leverett River (Hindshaw et al., 2014; Rickli et al., 2017). The mixing line between chlorite and feldspar/epidote in Ro4 is shown. The point where this line has the same $^{87}Sr/^{86}Sr$ value as the average of the river water samples (0.742435, Hindshaw et al., 2014) is defined as "Ro4-Leverett." The garnet end-member is defined in **Table 1**. Two carbonate end-members are defined based on acetic acid leaches of a felsic (carbF) and a mafic (carbM) rock from Akuliarusiarsuup Kuua River (AKR) (Andrews and Jacobson, 2018) and a δ^{26}Mg carbonate value of −3.2‰(Wimpenny et al., 2011). Mixing lines between Ro4-Leverett and carbonate (dashed lines) and Ro4-Leverett and garnet (solid line) are shown and assume congruent dissolution of each end-member. The numbers indicate the mass fraction of the garnet or carbonate end-member. Mineral abbreviations: Hbl, Hornblende; Chl, Chlorite; Cpx, Clinopyroxene; Grt, Garnet; Feld/Ep, K-feldspar, plagioclase, epidote mixture.

Further contributions from hornblende to the Mg budget in the river are likely based on the high fraction of Mg hosted in this mineral in the amphibolite rock samples (**Table 1**), high abundances of hornblende in catchment sediments (up to 9.5 vol.%, Rickli et al., 2017) and dissolved riverine Hf and Nd isotope compositions (Rickli et al., 2017). A contribution from hornblende would also be consistent with dissolved δ^{26}Mg and $^{87}Sr/^{86}Sr$ values since the range of δ^{26}Mg and $^{87}Sr/^{86}Sr$ values measured in hornblende separates encompasses those measured in the dissolved load (**Figure 5**).

Minerals derived from augen gneiss (**Figure 1**) could also contribute to dissolved Mg and Li in the Leverett River. Mg- and Li-rich minerals in the augen gneiss sample analyzed by Rickli et al. (2017) are biotite and hornblende (both 3 wt.%). Biotite was inferred to contribute to the dissolved load chemistry of the Russell Glacier river (Andrews and Jacobson, 2018; Auqué et al., 2019) and is found in river sediments from the Leverett catchment (<1.4 wt.%, Rickli et al., 2017). Mineral separates of the augen gneiss were not obtained and given the spread of δ^{7}Li and δ^{26}Mg in minerals from different rock samples is quite large (**Figure 4**), it is difficult to predict what the δ^{7}Li and δ^{26}Mg values of the Mg- and Li- rich augen gneiss minerals would be. Therefore, an accurate assessment of their contribution to the dissolved Mg and Li load in Leverett must await further data. We note though that Andrews and Jacobson (2018) concluded, based on $^{87}Sr/^{86}Sr$ and major element data, that the waters draining Point 660 catchment [where Auqué et al. (2019) collected their samples] drained a distinctly different lithology to Leverett, with a greater proportion of K-feldspar and/or biotite weathering compared to plagioclase weathering. Therefore, the contribution of biotite weathering to the dissolved load of Leverett River is expected to be lower compared to Russell.

The δ^{26}Mg values of river water samples previously measured in this region (**Figure 1**) were also explained as arising from a mixture of different mineral sources (Wimpenny et al., 2011). In the following discussion this sample set will be referred to as "Wimpenny's samples." In their study the authors suggested that low δ^{26}Mg values were arising from the presence of finely disseminated secondary carbonate in the catchment rocks. The presence of carbonate was not directly confirmed but was supported by elevated Ca/Na (up to 3.9 mol/mol) and Ca/Mg (up to 3.5 mol/mol) ratios in those water samples compared to a pure silicate end-member (Ca/Na = 0.5; Ca/Mg = 1.3, Wimpenny et al., 2011). Further, calcite has recently been detected in a glacier borehole sample from the AKR catchment (**Figure 1**, Harper et al., 2016) and the presence of disseminated calcite was inferred from element ratios of the fine fraction of till samples from north of Russell Glacier (Auqué et al., 2019). The estimated contribution of carbonate weathering to dissolved Mg was 2–7% (Wimpenny et al., 2011) and this estimate is consistent with other studies conducted in this region (Graly et al., 2014; Yde et al., 2014; Andrews and Jacobson, 2018).

We observe that the δ^{26}Mg values of Leverett River are ∼0.82‰ higher compared to Wimpenny's samples. This offset could be due to a difference in the contribution of carbonate weathering to dissolved Mg. In the Leverett River samples the molar Ca/Na ratios in river water (0.59 to 0.98, **Table 2**) are lower than those reported by Wimpenny et al. (2011) (1.07–3.88). This together with the lack of Mg-carbonate phases detected in the Leverett catchment rock and sediment samples could suggest that the contribution of carbonate weathering is lower in Leverett compared to the surrounding region. Since carbonate has low δ^{26}Mg values (−5.57 to −0.38‰, Teng, 2017) compared to the silicate rocks in this study (−0.20 to +0.09‰, **Table 1**), a smaller carbonate contribution in Leverett compared to Wimpenny's samples would result in higher dissolved δ^{26}Mg values, as observed.

In addition to carbonate, garnet also has lower δ^{26}Mg values compared to bulk silicate rocks and all the water samples (**Figure 3**, **Table 1**). The weathering rate of garnet (almandine) is predicted to be about two orders of magnitude faster than epidote and chlorite at the pH of the river waters (Palandri and Kharaka, 2004, and references therein) and therefore it is plausible that the dissolution of this mineral could impact on the dissolved load Mg isotopic composition. The higher Ca/Na ratios in Wimpenny's samples could similarly be explained by increased weathering from silicate minerals with high Ca/Na ratios, such as garnet

(Ca/Na molar ratio = 300), which are more abundant in the amphibolites compared to the orthogneisses (**Table 1**). Spatial differences in the relative contribution of garnet weathering may therefore also account for the difference in δ^{26}Mg values between the two datasets.

In order to test these two hypothesis (garnet and carbonate) we utilize $^{87}Sr/^{86}Sr$ ratios to assess if mixing between the proposed mineral sources fits the $^{87}Sr/^{86}Sr$ and δ^{26}Mg isotope data from the water samples (**Figure 5**). Wimpenny et al. (2011) did not analyse their samples for $^{87}Sr/^{86}Sr$ ratios, however data from similar sample sites along the AKR are available for 2014 and 2015 (Andrews and Jacobson, 2018). Compared to 2009, annual total and peak discharge were higher in 2014 and lower in 2015 (van As et al., 2017). No statistically significant change in $^{87}Sr/^{86}Sr$ ratios was observed during either melt season or between 2014 and 2015 at each site despite variations in discharge. Therefore, for the three sites common to both studies [GR1, GR2, GR8 in Wimpenny et al. (2011) and E, B, D in Andrews and Jacobson (2018)], we use the site-specific average $^{87}Sr/^{86}Sr$ value from 2014 and 2015. We assume that dissolved $^{87}Sr/^{86}Sr$ in Wimpenny's samples is controlled by the same reactions as inferred for Leverett, where minerals from orthogneiss Ro4 (chlorite, feldspar and epidote) appear to control the dissolved load composition. This assumption is supported by the overlapping range in $^{87}Sr/^{86}Sr$ ratios of AKR (0.7395–0.7462, sites E, B, D, Andrews and Jacobson, 2018) and Leverett water samples (0.7406–0.7455, **Figure 5**, Hindshaw et al., 2014).

We define one end-member (Ro4-Leverett) as the point where the feldspar/epidote—chlorite mixing line is at the average Leverett River $^{87}Sr/^{86}Sr$ ratio (0.742435, Hindshaw et al., 2014). We then assess the impact of mixing between Ro4-Leverett and solute sources with low δ^{26}Mg values: carbonate and garnet. There are no direct measurements of carbonate from this region, however Andrews and Jacobson (2018) performed an acetic acid leach of two rock samples (R05F and R05M) from the AKR catchment targeting carbonate. One sample was from a felsic rock (carbF, [Mg] =141 mg/kg, [Sr] = 3.1 mg/kg, $^{87}Sr/^{86}Sr$ = 0.71558) and the other from a mafic rock (carbM, [Mg] = 107 mg/kg, [Sr] = 0.7 mg/kg, $^{87}Sr/^{86}Sr$ = 0.72240). No δ^{26}Mg values exist for these samples and we therefore apply the same δ^{26}Mg value (–3.2‰) that (Wimpenny et al., 2011) assumed for carbonate. The mixing lines indicate that additional weathering of either carbonate or garnet could account for the lower δ^{26}Mg values observed in Wimpenny's samples compared to Leverett (**Figure 5**). For mixing between Ro4-Leverett and carbonate, the dissolved δ^{26}Mg values would require that carbonate weathering dominates in the AKR catchment (∼95 wt.% of the weathering substrate, **Figure 5**), which contradicts previous conclusions (Wimpenny et al., 2011; Andrews and Jacobson, 2018). In terms of garnet weathering, Rickli et al. (2017) estimated that, based on Nd and Hf isotopes, the contribution of garnet in Leverett was 2%. The δ^{26}Mg values measured in Leverett correspond to 0–6% garnet contribution, which is broadly consistent with the proposed mixing model for Nd and Hd isotope data. For Wimpenny's samples, the garnet mass fraction is ∼0.55 (**Figure 5**). Compared to Leverett, suspended sediments in AKR, QKR, and Watson River collected by Wimpenny et al. (2010) had higher Hf isotopic compositions (εHf = –38.12 ± 1.2, 1SD) compared to Leverett (εHf = –45.2 ± 1.2, 1SD) which was interpreted to reflect a combination of more garnet and less zircon in those suspended sediments (Rickli et al., 2017). Assuming that the suspended sediments provide a measure of the average lithology drained, the Hf isotope data would support the hypothesis that the lower δ^{26}Mg values in Wimpenny's samples could, at least in part, be caused by increased garnet weathering. However, the inferred difference in garnet abundance was estimated to be <1 wt.% and therefore unlikely to result in such a large difference in garnet contribution to the dissolved load as implied by the mixing proportions from **Figure 5**.

In summary, we cannot conclusively identify the origin of the offset between δ^{26}Mg values in Wimpenny's samples and Leverett River. Both increased garnet and carbonate weathering compared to Leverett may play a role, but neither on its own is consistent with constraints from mineral abundances and other geochemical data. However, there may be differences in lithology between Leverett and the other catchments (**Figure 1**), invalidating the assumption that the dissolution of orthogneiss Ro4 is the primary solute source to the dissolved load in Wimpenny's samples. Further data from bulk rock and mineral separate samples from the area where Wimpenny et al. (2011) collected their samples would be required to provide additional constraints on plausible weathering sources.

5.4. Fractionation Control on River Water Isotope Ratios

The δ^{7}Li values of Leverett River water samples cannot be reconciled with mixing between isotopically distinct mineral end-members (**Figure 6**). A fractionation process must therefore control river δ^{7}Li values and could also impact on δ^{26}Mg values.

The difference in the magnitude of fractionation ($\Delta^{7}Li_{water-sed}$) between the samples measured by Wimpenny et al. (2010) (∼20.4‰) and this study (∼14.3‰) could be due to a difference in lithology or the relative amount of Li lost from solution due to processes such as secondary mineral formation and adsorption. In the first scenario, the $\Delta^{7}Li_{water-sed}$ value would be constant but if the starting rock composition for Wimpenny's samples had a higher δ^{7}Li value compared to Leverett then the δ^{7}Li of the water samples would be correspondingly higher. There is only a minor difference in the δ^{7}Li values of the amphibolite (+6.8 to +8.3‰) and orthogneiss samples (+5.0 to +6.3‰, **Figure 3**). Similarly the range in rock δ^{7}Li values from this study (+5.0 to +8.3‰) overlaps with the range reported by Wimpenny et al. (2010) (+5.8 to +10.4‰). Theoretically, a hornblende with a high δ^{7}Li value such as that measured in Ro3 (+12.1‰) could dominate the dissolved load of the Wimpenny et al. (2010) samples, but that would be inconsistent with the Mg, Ca, and Sr isotope data (**Figure 5**, Hindshaw et al., 2014). As such it is unlikely that differences in the Li isotopic composition of the source rocks and minerals can account for the ∼6‰ difference in the δ^{7}Li values of the two sets of river water samples.

It is therefore more likely that the degree of fractionation between the two sample sets differs. Fractionation of Li isotopes

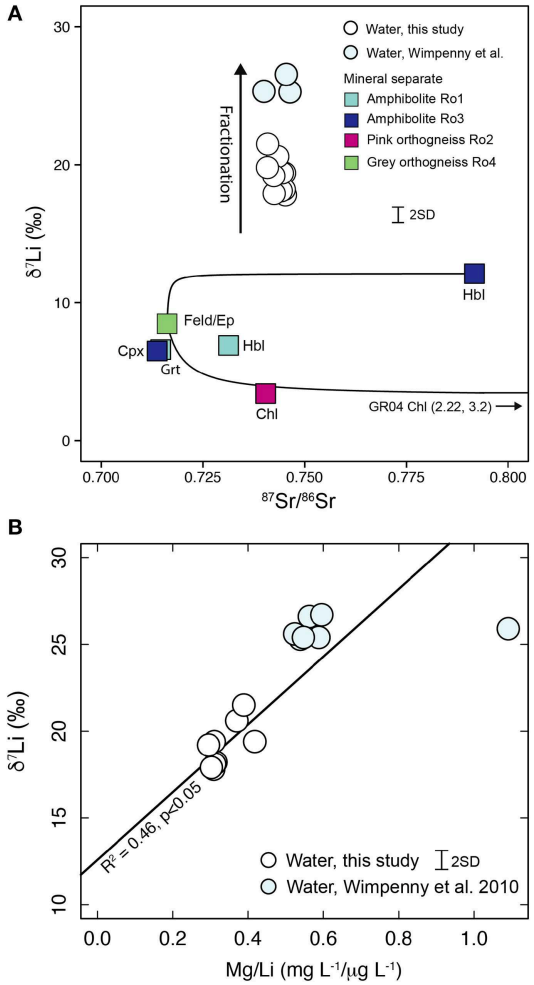

FIGURE 6 | (A) Mixing between the minerals of Ro4 (feldspar, epidote, and chlorite) cannot explain the δ^7Li values of water. Hornblende, the mineral with the highest δ^7Li values, also cannot account for the water δ^7Li values, even if it dominated the dissolved Li budget. Therefore, although some variation may be attributable to mineral source heterogeneity a fractionation process must also be occurring. Mineral abbreviations: Hbl, Hornblende; Chl, Chlorite; Cpx, Clinopyroxene; Grt, Garnet; Feld/Ep, K-feldspar, plagioclase, epidote mixture. Note that a change in the relative proportion of garnet weathering will have a negligible effect on δ^7Li ratios. **(B)** The water samples measured in this study have lower δ^7Li and Mg/Li values compared to Wimpenny et al. (2010). The lower Mg/Li values would be consistent either with a lower relative loss of Li compared to Mg or with a decreased contribution from garnet weathering (Mg/Li garnet = 2.1, **Figure 5B**). The solid line is the regression through Leverett River samples.

is attributed to two main processes: adsorption and secondary mineral formation (Huh et al., 2001; Pistiner and Henderson, 2003; Vigier et al., 2008). Both of these processes lead to an enrichment of ^{7}Li in the fluid. In high latitude environments adsorption rather than clay mineral formation likely controls dissolved Li isotopic compositions (Millot et al., 2010; Wimpenny et al., 2010). Evidence for the role of adsorption in glacierized catchments comes from the low δ^7Li values measured in a leach targeting Fe-oxyhydroxide phases in sediments from West Greenland (Wimpenny et al., 2010). Ilmenite ($FeTiO_3$) and magnetite (Fe_3O_4) are present in the Leverett River sediments and Phreeqc calculations indicate that water samples from the region are over-saturated in amorphous and crystalline iron oxide phases (Wimpenny et al., 2010; Hindshaw et al., 2014). Adsorption of metal cations (e.g., Li) onto these phases could therefore occur, particularly as adsorption is favored at basic pH due to a more negative surface charge compared to at neutral pH (Stumm and Morgan, 1996). Although Wimpenny et al. (2010) and Auqué et al. (2019) considered the formation of secondary clay minerals unlikely, smectite has been detected in sediments retrieved from glacier boreholes in this region (Graly et al., 2016). Smectite may originate from overridden soils (Yde et al., 2014; Carrivick et al., 2018) and adsorption onto the clay surface could also induce isotope fractionation (Pistiner and Henderson, 2003; Chan and Hein, 2007). Mineralogical and isotopic analysis of the clay-sized fraction of river sediment would be required to assess the role of clay minerals on dissolved δ^{26}Mg and δ^7Li.

The Mg/Li ratio is commonly used to assess the relative loss of Li in water samples (Dellinger et al., 2015). The Mg/Li mass ratios of the Wimpenny et al. (2010) samples are higher (0.6) compared to Leverett (0.3) potentially indicating increased loss of Li (**Figure 6B**). However, the Mg/Li ratio is also dependent on the relative proportion of garnet (Mg/Li = 2.1) weathering in these samples. The difference in lithology inferred from δ^{26}Mg values (**Figure 5**) implies that a common initial ion ratio cannot be assumed for all the water samples in this region and that the Mg/Li ratio is not a reliable measure of relative Li loss. Nevertheless, if we assume a single lithological source in the Leverett catchment, higher Mg/Li ratios are associated with higher δ^7Li values (**Figure 6B**), consistent with fractionation accompanying removal of Li from solution. We therefore consider it likely that the trend observed between δ^7Li and Mg/Li in the Leverett samples (**Figure 6B**) arises due to increased loss of Li. By extension, the higher δ^7Li values observed in the Wimpenny et al. (2010) samples are most likely due to greater fractionation (greater proportion of Li lost) rather than source differences.

If Li isotope fractionation in this region is caused by adsorption, as proposed by Wimpenny et al. (2010), then the difference in mineralogy of suspended sediments may impact the identity and availability of adsorption sites. Suspended sediments measured by Wimpenny et al. (2010) had Fe (3.68–5.07 wt.%) and Li (21.5–35.4 mg/kg) concentrations higher than those measured in Leverett (Fe = 3.46–3.92 wt.%; Li = 4.9–8.3 mg/kg, n = 6). The lower Fe and Li concentrations in Leverett suspended sediment may indicate fewer Fe oxides and a lower proportion of Li adsorbed, resulting in reduced fractionation compared to Wimpenny's samples.

The inferred fractionation of Li as a result of adsorption could imply that Mg isotopes are affected by the same process. Coupled Mg and Li isotope behavior has been observed in the Mackenzie River basin linked to secondary fractionation processes involving clay minerals (Tipper et al., 2012a). However, the range of dissolved δ^{26}Mg values in Leverett (–0.38 to –0.15‰) overlaps with those of the river sediments (–0.33 to –0.48, **Table 1**) suggesting negligible process-related fractionation. Rather, the Mg isotope data in Leverett can be adequately explained by

mixing between different mineral sources (**Figure 5**). Although the Mg isotope data in Wimpenny's samples is not fully compatible with mixing between mineral sources inferred for Leverett (section 5.3) we consider it unlikely that fractionation of Mg would occur in one catchment and not the other.

The samples collected downstream of the confluence of rivers draining Russell and Leverett glaciers would be expected to represent a mixture of water draining those glaciers. Transects of water samples from AKR show an increase in dissolved $^{87}Sr/^{86}Sr$ ratios downstream of the confluence with Leverett River (average increase = 0.006678, Andrews and Jacobson, 2018). This increase was attributed to the mixing of two end-members draining areas with different geology. We would therefore also expect the δ^7Li and δ^{26}Mg values downstream of the confluence (GR2 and GR8) to reflect a mixture between Leverett ($\delta^{26}Mg = -0.29‰$, $\delta^7Li = +19.2‰$) and GR1 ($\delta^{26}Mg = -1.04‰$, $\delta^7Li = +25.4‰$) (**Figure 1**). Yet, this is not what is observed. Rather the downstream δ^{26}Mg and δ^7Li values are within error of GR1 (Wimpenny et al., 2010, 2011). We do not have a good explanation for why the mixing signal for dissolved Li and Mg isotope values is absent. One source of uncertainty is that we are comparing water samples collected in different years (2006 and 2009) and the subglacial drainage pathways may not be identical from year to year (Lindbäck et al., 2015), potentially resulting in inter-annual variations in the dominant lithology being weathered for each glacier sub-catchment. For example, one year could have a higher proportion of solutes derived from mafic dykes compared to another year. Simultaneous measurements of water chemistry from both glaciers in the same melt-season would be needed to test this hypothesis.

6. CONCLUSIONS

Lithium and magnesium stable isotope ratios measured in a time series of water samples from Leverett Glacier display no systematic temporal variation and are affected by different processes. The Li isotope values of water samples are higher than bedrock, river sediment, and mineral separate measurements, implying a fractionation processes. A previous study concluded that dissolved lithium isotope values in this region were controlled by adsorption onto iron oxyhydroxide minerals (Wimpenny et al., 2010) and the same process is likely occurring in this catchment. In contrast, the δ^{26}Mg values of the dissolved load are within error of bedrock and river sediment measurements and would be consistent with the mixing of Mg derived from minerals contained in orthogneiss (chlorite, feldspar, and epidote), previously identified by radiogenic Ca and Sr measurements as being key sources to the dissolved load (Hindshaw et al., 2014). In addition there are likely contributions from garnet and hornblende. A previous study in this region (Qinnguata Kuussua (QKR) and Akuliarusiarsuup Kuua (AKR) rivers, Wimpenny et al., 2011), reported dissolved δ^{26}Mg values ~0.80‰ lower than those we measured in Leverett and concluded that there was a carbonate ($\delta^{26}Mg = -1$ to $-5‰$) contribution to Mg in the dissolved load. However, garnet also has low δ^{26}Mg value (–1.63‰), and could also contribute to dissolved Mg in these samples. Mixing calculations between a "Leverett" end-member and either carbonate or garnet suggest that whilst the weathering of both minerals could account for the difference in δ^{26}Mg values between the two data sets, the inferred mixing proportions are incompatible with other geochemical data. It is likely that the mineral data from Leverett does not capture all mineral sources for the AQR and QKR catchments due to small differences in lithology.

In the context of the carbon cycle it is crucial to determine whether Mg (and Ca) derive from carbonate or silicate weathering. This study highlights that certain silicate minerals can have δ^{26}Mg values in the same range as carbonate minerals, emphasizing that source rock mineral characterization is an essential step in the interpretation of dissolved stable isotope ratios.

DATA AVAILABILITY STATEMENT

All datasets generated for this study are included in the manuscript or are available in the referenced companion manuscripts.

AUTHOR CONTRIBUTIONS

RH designed the project and conducted the fieldwork together with JR. JL collected element and abundance data on mineral separates and RH analyzed samples for Li and Mg isotope ratios. All authors contributed to the interpretation of the results and the writing of the article.

FUNDING

This work was funded by a SNF fellowship (127764) and Marie-Curie Fellowship (Project No. 253117) to JR and an ETH Research Grant (no. 04/06-3) and NERC Standard Grant (NE/M001865/1) to RH. JL acknowledges support from a Swiss National Science Foundation (SNSF) Ambizione grant.

REFERENCES

AMAP (2017). *Snow, Water, Ice and Permafrost in the Arctic (SWIPA) 2017*. Oslo: Arctic Monitoring and Assessment Programme (AMAP).

Anderson, S. P., Drever, J. I., and Humphrey, N. F. (1997). Chemical weathering in glacial environments. *Geology* 25, 399–402. doi: 10.1130/0091-7613(1997)025<0399:CWIGE>2.3.CO;2

Andrews, M. G., and Jacobson, A. D. (2018). Controls on the solute geochemistry of subglacial discharge from the Russell Glacier, Greenland Ice Sheet determined by radiogenic and stable Sr isotope ratios. *Geochim. Cosmochim. Acta* 239, 312–329. doi: 10.1016/j.gca.2018.08.004

Auqué, L. F., Puigdomenech, I., Tullborg, E.-L., Gimeno, M. J., Grodzinsky, K., and Hogmalm, K. J. (2019). Chemical weathering in a moraine at the ice sheet margin at Kangerlussuaq, western Greenland. *Arct. Antarct. Alp. Res.* 51, 440–459. doi: 10.1080/15230430.2019.1660125

Barnes, E. M., Weis, D., and Groat, L. A. (2012). Significant Li isotope fractionation in geochemically evolved rare element-bearing pegmatites from

the Little Nahanni Pegmatite Group, NWT, Canada. *Lithos* 132–133, 21–36. doi: 10.1016/j.lithos.2011.11.014

Bartholomew, I., Nienow, P., Sole, A., Mair, D., Cowton, T., Palmer, S., et al. (2011). Supraglacial forcing of subglacial drainage in the ablation zone of the Greenland ice sheet. *Geophys. Res. Lett.* 38:L08502. doi: 10.1029/2011GL047063

Berner, R. A., Lasaga, A. C., and Garrels, R. M. (1983). The carbonate-silicate geochemical cycle and its effect on atmospheric carbon dioxide over the past 100 million years. *Am. J. Sci.* 283, 641–683. doi: 10.2475/ajs.283.7.641

Bhatia, M. P., Das, S. B., Xu, L., Charette, M. A., Wadham, J. L., and Kujawinski, E. B. (2013). Organic carbon export from the Greenland ice sheet. *Geochim. Cosmochim. Acta* 109, 329–344. doi: 10.1016/j.gca.2013.02.006

Blum, J. D., and Erel, Y. (1997). Rb-Sr isotope systematics of a granitic soil chronosequence: the importance of biotite weathering. *Geochim. Cosmochim. Acta* 61, 3193–3204. doi: 10.1016/S0016-7037(97)00148-8

Blum, J. D., Erel, Y., and Brown, K. (1994). $^{87}Sr/^{86}Sr$ ratios of Sierra Nevada stream waters: implications for relative mineral weathering rates. *Geochim. Cosmochim. Acta* 58, 5019–5025. doi: 10.1016/S0016-7037(05)80014-6

Brown, M., Friend, C. R. L., McGregor, V. R., and Perkins, W. T. (1981). The late Archaean Qôrqut granite complex of Southern West Greenland. *J. Geophys. Res.* 86, 10617–10632. doi: 10.1029/JB086iB11p10617

Bullen, T. D., and Bailey, S. W. (2005). Identifying calcium sources at an acid deposition-impacted spruce forest: a strontium isotope, alkaline earth element multi-tracer approach. *Biogeochemistry* 74, 63–99. doi: 10.1007/s10533-004-2619-z

Cadman, A. C., Tarney, J., Bridgewater, D., Mengel, F., Whitehouse, M. J., and Windley, B. F. (2001). The petrogenesis of the Kangâmiut dyke swarm, W. Greenland. *Precambrian Res.* 105, 183–203. doi: 10.1016/S0301-9268(00)00111-X

Carignan, J., Vigier, N., and Millot, R. (2007). Three secondary reference materials for lithium isotope measurements: Li7-N, Li6-N and LiCl-N solutions. *Geostand. Geoanal. Res.* 31, 7–12. doi: 10.1111/j.1751-908X.2007.00833.x

Carrivick, J. L., Yde, J. C., Knudsen, N. T., and Kronborg, C. (2018). Ice-dammed lake and ice-margin evolution during the Holocene in the Kangerlussuaq area of west Greenland. *Arct. Antarct. Alp. Res.* 50:e1420854. doi: 10.1080/15230430.2017.1420854

Chan, L.-H., and Hein, J. R. (2007). Lithium contents and isotopic compositions of ferromanganese deposits from the global ocean. *Deep Sea Res. II* 54, 1147–1162. doi: 10.1016/j.dsr2.2007.04.003

Chandler, D. M., Wadham, J. L., Lis, G. P., Cowton, T., Sole, A., Bartholomew, I., et al. (2013). Evolution of the subglacial drainage system beneath the Greenland Ice Sheet revealed by tracers. *Nat. Geosci.* 6, 195–198. doi: 10.1038/ngeo1737

Chapela Lara, M., Buss, H. L., Pogge von Strandmann, P. A. E., Schuessler, J., and Moore, O. W. (2017). The influence of critical zone processes on the Mg isotope budget in a tropical, highly weathered andesitic catchment. *Geochim. Cosmochim. Acta* 202, 77–100. doi: 10.1016/j.gca.2016.12.032

Chen, L.-M., Teng, F. Z., Song, X.-Y., Hu, R.-Z., Yu, S.-Y., Zhu, D., et al. (2018). Magnesium isotopic evidence for chemical disequilibrium among cumulus minerals in layered mafic intrusion. *Earth Planet. Sci. Lett.* 487, 74–83. doi: 10.1016/j.epsl.2018.01.036

Clergue, C., Dellinger, M., Buss, H. L., Gaillardet, J., Benedetti, M. F., and Dessert, C. (2015). Influence of atmospheric deposits and secondary minerals on Li isotopes budget in a highly weathered catchment, Guadeloupe (Lesser Antilles). *Chem. Geol.* 414, 28–41. doi: 10.1016/j.chemgeo.2015.08.015

Cussen, E. J. (2010). Structure and ionic conductivity in lithium garnets. *J. Mater. Chem.* 20, 5167–5173. doi: 10.1039/b925553b

Dellinger, M., Gaillardet, J., Bouchez, J., Calmels, D., Louvat, P., Dosseto, A., et al. (2015). Riverine Li isotope fractionation in the Amazon River basin controlled by the weathering regimes. *Geochim. Cosmochim. Acta* 164, 71–93. doi: 10.1016/j.gca.2015.04.042

Engström, J., and Klint, K. E. S. (2014). Continental collision structures and post-orogenic geological histroy of the Kangerlussuaq are in the southern part of the Nagssugtoqidian Orogen, Central West Greenland. *Geosciences* 4, 316–334. doi: 10.3390/geosciences4040316

Escher, A. (1971). *Geological Map of Greenland, 1:500 000, Søndre Strømfjord - Nûgssuaq, Sheet 3*. Copenhagen: Geological Survey of Greenland.

Escher, A., Sørensen, K., and Zeck, H. P. (1976). "Nagssugtoqidian mobile belt in West Greenland," in *Geology of Greenland*, eds A. Escher and W. S. Watt (Copenhagen: Grønlands Geologiske Undersøgelse), 76–95.

Gaillardet, J., Dupré, B., Louvat, P., and Allègre, C. J. (1999). Gobal silicate weathering and CO_2 consumption rates deduced from the chemistry of large rivers. *Chem. Geol.* 159, 3–30. doi: 10.1016/S0009-2541(99)00031-5

Garrels, R. M., and Howard, P. (1957). Reactions of feldspar and mica with water at low temperature and pressure. *Clay Clay Miner.* 6, 68–88.

Graly, J. A., Humphrey, N. F., and Harper, J. T. (2016). Chemical depletion of sediment under the Greenland Ice Sheet. *Earth Surf. Process. Landforms* 41, 1922–1936. doi: 10.1002/esp.3960

Graly, J. A., Humphrey, N. F., Landowski, C. M., and Harper, J. (2014). Chemical weathering under the Greenland Ice Sheet. *Geology* 42, 551–554. doi: 10.1130/G35370.1

Hanna, E., Mernild, S. H., Cappelen, J., and Steffen, K. (2012). Recent warming in Greenland in a long-term instrumental (1881-2012) climatic context: I. evalulation of surface air temperature records. *Environ. Res. Lett.* 7:045404. doi: 10.1088/1748-9326/7/4/045404

Harper, J., Hubbard, A., Ruskeeniemi, T., Claesson Liljedahl, L., Kontula, A., Hobbs, M., et al. (2016). *The Greenland Analogue Project: Data and Processes*. Tech. Rep. R-14-13, Svensk Kärnbränslehantering AB, Stockholm.

Hawkings, J., Wadham, J., Tranter, M., Telling, J., Bagshaw, E., Beaton, A., et al. (2016). The Greenland Ice Sheet as a hotspot of phosphorus weathering and export in the Arctic. *Glob. Biogeochem. Cycles* 30, 191–210. doi: 10.1002/2015GB005237

Hawkings, J. R., Wadham, J. L., Benning, L. G., Hendry, K. R., Tranter, M., Tedstone, A., et al. (2017). Ice sheets as a missing source of silica to the polar oceans. *Nat. Commun.* 8:4198. doi: 10.1038/ncomms14198

Hawkings, J. R., Wadham, J. L., Tranter, M., Raiswell, R., Benning, L. G., Statham, P. J., et al. (2014). Ice sheets as a significant source of highly reactive nanoparticulate iron to the oceans. *Nat. Commun.* 5:3929. doi: 10.1038/ncomms4929

Henriksen, N., Higgins, A. K., Kalsbeek, F., and Pulvertaft, T. C. R. (2000). Greenland from Archaean to quaternary: descriptive text to the geological map of Greenland, 1:2 500 000. *Geol. Greenland Surv. Bull.* 185, 1–126. Available online at: https://eng.geus.dk/products-services-facilities/publications/geus-bulletin/geology-of-greenland-survey-bulletin/bulletin-185/

Hindshaw, R. S., Aciego, S. M., and Tipper, E. T. (2018). Li and U isotopes as a potential tool for monitoring active layer deepening in permafrost dominated catchments. *Front. Earth Sci.* 6:102. doi: 10.3389/feart.2018.00102

Hindshaw, R. S., Rickli, J., Leuthold, J., Wadham, J., and Bourdon, B. (2014). Identifying weathering sources and processes in an outlet glacier of the Greenland Ice Sheet using Ca and Sr isotope ratios. *Geochim. Cosmochim. Acta* 145, 50–71. doi: 10.1016/j.gca.2014.09.016

Hindshaw, R. S., Tipper, E. T., Reynolds, B. C., Lemarchand, E., Wiederhold, J. G., Magnusson, J., et al. (2011). Hydrological control of stream water chemistry in a glacial catchment (Damma Glacier, Switzerland). *Chem. Geol.* 285, 215–230. doi: 10.1016/j.chemgeo.2011.04.012

Hopwood, M. J., Bacon, S., Arendt, K., Connelly, D. P., and Statham, P. J. (2015). Glacial meltwater from Greeland is not likely to be an important source of Fe to the North Atlantic. *Biogeochemistry* 124, 1–11. doi: 10.1007/s10533-015-0091-6

Hu, Y., Teng, F. Z., Zhang, H.-F., Xiao, Y., and Su, B.-X. (2016). Metasomatism-induced mantle magnesium isotopic heterogeneity: evidence from pyroxenites. *Geochim. Cosmochim. Acta* 185, 88–111. doi: 10.1016/j.gca.2015.11.001

Huang, F., Chen, L., Wu, Z., and Wang, W. (2013). First-principles calculations of equilibrium Mg isotope fractionations between garnet, clinopyroxene, orthopyroxene, and olivine: implications for Mg isotope thermometry. *Earth Planet. Sci. Lett.* 367, 61–70. doi: 10.1016/j.epsl.2013.02.025

Huh, Y., Chan, L.-H., and Edmond, J. M. (2001). Lithium isotopes as a probe of weathering processes: Orinoco river. *Earth Planet. Sci. Lett.* 194, 189–199. doi: 10.1016/S0012-821X(01)00523-4

Huh, Y., Panteleyev, G., Babich, D., Zaitsev, A., and Edmond, J. M. (1998). The fluvial geochemistry of the rivers of Eastern Siberia: II. Tributaries of the Lena, Omoloy, Yana, Indigirka, Kolyma, and Anadyr draining the collisional/accretionary zone of the Verkhoyansk and Cherskiy ranges. *Geochim. Cosmochim. Acta* 62, 2053–2075. doi: 10.1016/S0016-7037(98)00127-6

James, R. H., and Palmer, M. R. (2000). The lithium isotope composition of international rock standards. *Chem. Geol.* 166, 319–326. doi: 10.1016/S0009-2541(99)00217-X

Johansson, E., Gustafsson, L.-G., Berglund, S., Lindborg, T., Selroos, J.-O., Liljedahl, L. C., et al. (2015). Data evaluation and numerical modeling of hydrological interactions between active layer, lake and talik in a permafrost catchment, Western Greenland. *J. Hydrol.* 527, 688–703. doi: 10.1016/j.jhydrol.2015.05.026

Kimmig, S. R., Holmden, C., and Bélanger, N. (2018). Biogeochemical cycling of Mg and its isotopes in a sugar maple forest in Québec. *Geochim. Cosmochim. Acta* 230, 60–82. doi: 10.1016/j.gca.2018.03.020

Li, W.-Y., Teng, F.-Z., Xiao, Y., Gu, H.-O., Zha, X.-P., and Huang, J. (2016). Empirical calibration of the clinopyroxene-garnet magnesium isotope geothermometer and implications. *Contrib. Mineral. Petrol.* 171, 61. doi: 10.1007/s00410-016-1269-1

Li, W. Y., Teng, F. Z., Ke, S., Rudnick, R. L., Gao, S., Wu, F. Y., et al. (2010). Heterogeneous magnseium isotopic composition of the upper continental crust. *Geochim. Cosmochim. Acta* 74, 6867–6884. doi: 10.1016/j.gca.2010.08.030

Lindbäck, K., Pettersson, R., Hubbard, A. L., Doyle, S. H., van As, D., Mikkelsen, A. B., et al. (2015). Subglacial water drainage, storage, and piracy beneath the Greenland ice sheet. *Geophys. Res. Lett.* 42, 7606–7614. doi: 10.1002/2015GL065393

Liu, S., Li, Y., Liu, J., Ju, Y., Liu, J., Yang, Z., et al. (2018). Equilibrium lithium isotope fractionation in Li-bearing minerals. *Geochim. Cosmochim. Acta* 235, 360–375. doi: 10.1016/j.gca.2018.05.029

Liu, S.-A., Teng, F.-Z., He, Y., Ke, S., and Li, S. (2010). Investigation of magnesium isotope fractionation during granite differentiation: implication for Mg isotopic composition of the continental crust. *Earth Planet. Sci. Lett.* 297, 646–654. doi: 10.1016/j.epsl.2010.07.019

Liu, X.-M., Rudnick, R. L., Hier-Majumder, S., and Sirbescu, M.-L. C. (2010). Processes controlling lithium isotopic distribution in contact aureoles: a case study of the Florence County pegmatites, Wisconsin. *Geochem. Geophys. Geosys.* 11:Q08014. doi: 10.1029/2010GC003063

Marks, M. A. W., Rudnick, R. L., McCammon, C., Vennemann, T., and Markl, G. (2007). Arrested kinetic Li isotope fractionation at the margin of the Ilímaussaq complex, South Greenland: evidence for open-system processes during final cooling of peralkaline igneous rocks. *Chem. Geol.* 246, 207–230. doi: 10.1016/j.chemgeo.2007.10.001

Mazza, D. (1988). Remarks on a ternary phase in the La_2O_3-Me_2O_5-Li_2O system (Me = Nb, Ta). *Mater. Lett.* 7, 205–207. doi: 10.1016/0167-577X(88)90011-0

Meire, L., Meire, P., Struyf, E., Krawczyk, D. W., Arendt, K. E., Yde, J. C., et al. (2016). High export of dissolved silica from the Greenland Ice Sheet. *Geophys. Res. Lett.* 43, 9173–9182. doi: 10.1002/2016GL070191

Mernild, S. H., Hanna, E., McConnell, M., Adn Sigl, J. R., Beckerman, A. P., Yde, J. C., et al. (2015). Greenland precipitation trends in a long-term instrumental climate context (1890-2012): evaluation of coastal and ice core records. *Int. J. Climatol.* 35, 303–320. doi: 10.1002/joc.3986

Millot, R., Vigier, N., and Gaillardet, J. (2010). Behaviour of lithium and its isotopes during weathering in the Mackenzie Basin, Canada. *Geochim. Cosmochim. Acta* 74, 3897–3912. doi: 10.1016/j.gca.2010.04.025

Misra, S., and Froelich, P. N. (2012). Lithium isotope history of Cenozoic seawater: changes in silicate weathering and reverse weathering. *Science* 335, 818–823. doi: 10.1126/science.1214697

Neukampf, J., Ellis, B. S., Magna, T., Laurent, O., and Bachmann, O. (2019). Partitioning and isotopic fractionation of lithium in mineral phases of hot, dry rhyolites: the case of the Mesa Falls Tuff, Yellowstone. *Chem. Geol.* 506, 175–186. doi: 10.1016/j.chemgeo.2018.12.031

Nezat, C. A., Blum, J. D., and Driscoll, C. T. (2010). Patterns of Ca/Sr and $^{87}Sr/^{86}Sr$ variation before and after a whole watershed $CaSiO_3$ addition at the Hubbard Brook Experimental Forest, USA. *Geochim. Cosmochim. Acta* 74, 3129–3142. doi: 10.1016/j.gca.2010.03.013

Nutman, A. P., Hiess, J., and Friend, C. R. L. (2010). Setting of the 2560 Ma Qorqut granite complex in the Archean crustal evolution of southern West Greenland. *Am. J. Sci.* 310, 1081–1114. doi: 10.2475/09.2010.12

O'Callaghan, M. P., Powell, A. S., Titman, J. J., Chen, G. Z., and Cussen, E. J. (2008). Switching on fast lithium ion conductivity in garnets: the structure and transport properties of $Li_{3+x}Nd_3Te_{2-x}Sb_xO_{12}$. *Chem. Mater.* 20, 2360–2369. doi: 10.1021/cm703677q

Oi, T., Nomura, M., Musashi, M., Ossaka, T., Okamoto, M., and Kakihana, H. (1989). Boron isotopic compositions of some boron minerals. *Geochim. Cosmochim. Acta* 53, 3189–3195. doi: 10.1016/0016-7037(89)90099-9

Oliva, P., Dupré, B., Martin, F., and Viers, J. (2004). The role of trace minerals in chemical weathering in a high-elevation granitic watershed (Estibère, France): chemical and mineralogical evidence. *Geochim. Cosmochim. Acta* 68, 2223–2244. doi: 10.1016/j.gca.2003.10.043

Palandri, J. L., and Kharaka, Y. K. (2004). *A Compilation of Rate Parameters of Water-Mineral Interaction Kinetics for Application for Geochemical Modeling.* U.S.G.S., Open File Report 2004-1068.

Penniston-Dorland, S., Liu, X.-M., and Rudnick, R. L. (2017). Lithium isotope geochemistry. *Rev. Mineral. Geochem.* 82, 165–217. doi: 10.1515/9783110545630-007

Phan, T. T., Capo, R. C., Stewart, B. W., Macpherson, G. L., Rowan, E. L., and Hammack, R. W. (2016). Factors controlling Li concentration and isotopic composition in formation waters and host rocks of Marcellus Shale, Appalachian Basin. *Chem. Geol.* 420, 162–179. doi: 10.1016/j.chemgeo.2015.11.003

Pistiner, J. S., and Henderson, G. M. (2003). Lithium-isotope fractionation during continental weathering processes. *Earth Planet. Sci. Lett.* 214, 327–339. doi: 10.1016/S0012-821X(03)00348-0

Pogge von Strandmann, P. A. E., Dohmen, R., Marschall, H. R., Schumacher, J. C., and Elliott, T. (2015). Extreme magnesium isotope fractionation at outcrop scale records the mechanism and rate at which reaction fronts advance. *J. Petrol.* 56, 33–58. doi: 10.1093/petrology/egu070

Pogge von Strandmann, P. A. E., Elliott, T., Marschall, H. R., Coath, C., Lai, Y.-J., Jeffcoate, A. B., et al. (2011). Variations of Li and Mg isotope ratios in bulk chondrites and mantle xenoliths. *Geochim. Cosmochim. Acta* 75, 5247–5268. doi: 10.1016/j.gca.2011.06.026

Raiswell, R., Tranter, M., Benning, L. G., Siegert, M., De'ath, R., Huybrechts, P., et al. (2006). Contributions from glacially derived sediment to the global iron (oxyhydr)oxide cycle: implications for iron delivery to the oceans. *Geochim. Cosmochim. Acta* 70, 2765–2780. doi: 10.1016/j.gca.2005.12.027

Rennermalm, A. K., Smith, L. C., Chu, V. W., Forster, R. R., Box, J. E., and Hagedorn, B. (2012). Proglacial river stage, discharge, and temperature datasets from the Akuliarusiarsupp Kuua River northern tributary, Soutwest Greenland, 2008-2011. *Earth Syst. Sci. Data* 4, 1–12. doi: 10.5194/essd-4-1-2012

Rettenwander, D., Wagner, R., Langer, J., Maier, M. E., Wilkening, M., and Amthauer, G. (2016). Crystal chemistry of "$Li_7La_3Zr_2O_12$" garnet doped with Al, Ga, and Fe: a short review on local structures as revealed by NMR and Mößbauer spectroscopy studies. *Eur. J. Mineral.* 28, 619–629. doi: 10.1127/ejm/2016/0028-2543

Rickli, J., Hindshaw, R. S., Leuthold, J., Wadham, J. L., Burton, K. W., and Vance, D. (2017). Impact of glacial activity on the weathering of Hf isotopes - observations from Southwest Greenland. *Geochim. Cosmochim. Acta* 215, 295–316. doi: 10.1016/j.gca.2017.08.005

Rosner, M., Ball, L., Peucker-Ehrenbrink, B., Blusztajn, J., Bach, W., and Erzinger, J. (2007). A simplified, accurate and fast method for lithium isotope analysis of rocks and fluids, and δ^7Li values of seawater and rock reference materials. *Geostand. Geoanal. Res.* 31, 77–88. doi: 10.1111/j.1751-908X.2007.00843.x

Ryu, J. S., Jacobson, A. D., Holmden, C., Lundstrom, C., and Zhang, Z. (2011). The major ion, $\delta^{44/40}$Ca, $\delta^{44/42}$Ca, and $\delta^{26/24}$Mg geochemistry of granite weathering at pH=1 and T=25°C: power-law processes and the relative reactivity of minerals. *Geochim. Cosmochim. Acta* 75, 6004–6026. doi: 10.1016/j.gca.2011.07.025

Sauzéat, L., Rudnick, R. L., Chauvel, C., Garçon, M., and Tang, M. (2015). New perspectives on the Li isotopic composition of the upper continental crust and its weathering signature. *Earth Planet. Sci. Lett.* 428, 181–192. doi: 10.1016/j.epsl.2015.07.032

Schauble, E. A. (2004). "Applying stable isotope fractionation theory to new systems," in *Geochemistry of Non-traditional Stable Isotopes*, Vol. 55 of *Reviews in Mineralogy & Geochemistry,* eds C. M. Johnson, B. L. Beard, and F. Albarède (Washington, DC: Mineralogical Society of America), 65–111.

Schauble, E. A. (2011). First-principles calculations of equilibrium magnesium isotope fractionation in silicate, oxide, carbonate and hexaaquamagnesium(2+) crystals. *Geochim. Cosmochim. Acta* 75, 844–869. doi: 10.1016/j.gca.2010.09.044

Sharp, M., Tranter, M., Brown, G. H., and Skidmore, M. (1995). Rates of chemical denudation and CO_2 drawdown in a glacier-covered alpine catchment. *Geology* 23, 61–64. doi: 10.1130/0091-7613(1995)023<0061:ROCDAC>2.3.CO;2

Shen, B., Jacobsen, B., Lee, C.-T. A., Yin, Q.-Z., and Morton, D. M. (2009). The Mg isotopic systematics of granitoids in continental arcs and implications for the role of chemical weathering in crust formation. *Proc. Natl. Acad. Sci. U.S.A.* 106, 20652–20657. doi: 10.1073/pnas.0910663106

Stracke, A., Tipper, E. T., Klemme, S., and Bizimis, M. (2018). Mg isotope systematics during magmatic processes: Inter-mineral fractionation in mafic to ultramafic Hawaiian xenoliths. *Geochim. Cosmochim. Acta* 226, 192–205. doi: 10.1016/j.gca.2018.02.002

Stumm, W., and Morgan, J. J. (1996). *Aquatic Chemistry: Chemical Equilibria and Rates in Natural Waters, 3rd Edn.* New York, NY: Wiley.

Sullivan, P. L., Ma, L., West, N., Jin, L., Karwan, D. L., Noireaux, J., et al. (2016). CZ-tope at Suquehanna Shale Hills CZO: synthesizing multiple isotope proxies to elucidate Critical Zone processes across timescales in a temperate forested landscape. *Chem. Geol.* 445, 103–119. doi: 10.1016/j.chemgeo.2016.05.012

Teng, F.-Z. (2017). Magnesium isotope geochemistry. *Rev. Mineral. Geochem.* 82, 219–287. doi: 10.2138/rmg.2017.82.7

Teng, F.-Z., Li, W.-Y., Ke, S., Yang, W., Liu, S.-A., Sedaghatpour, F., et al. (2015). Magnesium isotopic compositions of international geological reference materials. *Geostand. Geoanal. Res.* 39, 329–339. doi: 10.1111/j.1751-908X.2014.00326.x

Teng, F.-Z., Li, W.-Y., Rudnick, R. L., and Gardner, L. R. (2010). Contrasting lithium and magnesium isotope fractionation during continental weathering. *Earth Planet. Sci. Lett.* 300, 63–71. doi: 10.1016/j.epsl.2010.09.036

Teng, F.-Z., McDonough, W. F., Rudnick, R. L., Dalpé, C., Tomascak, P. B., Chappell, B. W., et al. (2004). Lithium isotopic composition and concentration of the upper continental crust. *Geochim. Cosmochim. Acta* 68, 4167–4178. doi: 10.1016/j.gca.2004.03.031

Teng, F.-Z., McDonough, W. F., Rudnick, R. L., Walker, R. J., and Sirbescu, M.-L. C. (2006). Lithium isotopic systematics of granites and pegmatites from the Black Hills, South Dakota. *Am. Mineral.* 91, 1488–1498. doi: 10.2138/am.2006.2083

Tipper, E. T., Bickle, M. J., Galy, A., West, A. J., Pomiès, C., and Chapman, H. J. (2006). The short term climatic sensitivity of carbonate and silicate weathering fluxes: insight from seasonal variations in river chemistry. *Geochim. Cosmochim. Acta* 70, 2737–2754. doi: 10.1016/j.gca.2006.03.005

Tipper, E. T., Calmels, D., Gaillardet, J., Louvat, P., Capmas, F., and Dubacq, B. (2012a). Positive correlation between Li and Mg isotope ratios in the river waters of the Mackenzie Basin challenges the interpretation of apparent isotopic fractionation during weathering. *Earth Planet. Sci. Lett.* 333-334, 35–45. doi: 10.1016/j.epsl.2012.04.023

Tipper, E. T., Lemarchand, E., Hindshaw, R. S., Reynolds, B. C., and Bourdon, B. (2012b). Seasonal sensitivity of weathering processes: hints from magnesium isotopes in a glacial stream. *Chem. Geol.* 312–313, 80–92. doi: 10.1016/j.chemgeo.2012.04.002

Tipper, E. T., Louvat, P., Capmas, F., Galy, A., and Gaillardet, J. (2008). Accuracy of stable Mg and Ca isotope data obtained by MC-ICP-MS using the standard addition method. *Chem. Geol.* 257, 65–75. doi: 10.1016/j.chemgeo.2008.08.016

Tomascak, P. B., Magna, T., and Dohmen, R. (2016). "The surficial realm: low temperature geochemistry of lithium," in *Advances in Lithium Isotope Geochemistry*, eds P. B. Tomascak, T. Magna, and R. Dohmen (Cham: Springer), 157–189.

Torres, M. A., Moosdorf, N., Hartmann, J., Adkins, J. F., and West, A. J. (2017). Glacial weathering, sulfide oxidation, and global carbon cycle feedbacks. *Proc. Natl. Acad. Sci. U.S.A.* 114, 8716–8721. doi: 10.1073/pnas.1702953114

Tranter, M. (2003). "Geochemical weathering in glacial and proglacial environments," in *Treatise on Geochemistry, Vol. 5: Surface and Ground Water, Weathering and Soils*, eds H. D. Holland and K. K. Turekian (Oxford: Elsevier), 189–205.

Tranter, M., Sharp, M. J., Lamb, H. R., Brown, G. H., Hubbard, B. P., and Willis, I. C. (2002). Geochemical weathering at the bed of Haut Glacier d'Arolla, Switzerland - a new model. *Hydrol. Process.* 16, 959–993. doi: 10.1002/hyp.309

van As, D., Mikkelsen, A. B., Nielsen, M. H., Box, J. E., Liljedahl, L. C., Lindbäck, K., et al. (2017). Hypsometric amplification and routing moderation of Greenland ice sheet meltwater release. *Cryosphere* 11, 1371–1386. doi: 10.5194/tc-11-1371-2017

Van Gool, J. A. M., Connelly, J. N., Marker, M., and Mengel, F. C. (2002). The Nagssugtoqidian Orogen of West Greenland: tectonic evolution and regional correlations from a West Greenland perspective. *Can J. Earth Sci.* 39, 665–686. doi: 10.1139/e02-027

Van Tatenhove, F. G. M. (1996). Changes in morphology at the margin of the Greenland ice sheet (Leverett Glacier), in the period 1943-1992: a quantitative analysis. *Earth Surf. Process. Landforms* 21, 797–816. doi: 10.1002/(SICI)1096-9837(199609)21:9<797::AID-ESP617>3.0.CO;2-2

Vance, D., Teagle, D. A. H., and Foster, G. L. (2009). Variable Quaternary chemical weathering fluxes and imbalances in marine geochemical budgets. *Nature* 458, 493–496. doi: 10.1038/nature07828

Vigier, N., Decarreau, A., Millot, R., Carignan, J., Petit, S., and France-Lanord, C. (2008). Quantifying Li isotope fractionation during smectite formation and implications for the Li cycle. *Geochim. Cosmochim. Acta* 72, 780–792. doi: 10.1016/j.gca.2007.11.011

Walker, J. C. G., Hays, P. B., and Kasting, J. F. (1981). A negative feedback mechanism for the long term stabilization of Earth's surface temperature. *J. Geophys. Res.* 86, 9776–9782. doi: 10.1029/JC086iC10p09776

Wang, S.-J., Teng, F. Z., Li, S.-G., and Hong, J.-A. (2014). Magnesium isotope systematics of mafic rocks during continental subduction. *Geochim. Cosmochim. Acta* 143, 34–48. doi: 10.1016/j.gca.2014.03.029

Wang, S.-J., Teng, F. Z., Williams, H. M., and Li, S.-G. (2012). Magnesium isotope variations in cratonic eclogites: origins and implications. *Earth Planet. Sci. Lett.* 359-360, 219–226. doi: 10.1016/j.epsl.2012.10.016

Wedepohl, K. H. (1995). The composition of the continental crust. *Geochim. Cosmochim. Acta* 59, 1217–1232. doi: 10.1016/0016-7037(95)00038-2

Wehrmann, L. M., Formolo, M. J., Owens, J. D., Raiswell, R., Ferdelman, T. G., Riedinger, N., et al. (2014). Iron and manganese speciation and cycling in glacially influenced high-latitude fjord sediments (West Spitsbergen, Svalbard): evidence for a benthic recycling-transport mechanism. *Geochim. Cosmochim. Acta* 141, 628–655. doi: 10.1016/j.gca.2014.06.007

Wimpenny, J., Burton, K. W., James, R. H., Gannoun, A., Mokadem, F., and Gíslason, S. R. (2011). The behaviour of magnesium and its isotopes during glacial weathering in an ancient shield terrain in West Greenland. *Earth Planet. Sci. Lett.* 304, 260–269. doi: 10.1016/j.epsl.2011.02.008

Wimpenny, J., Colla, C. A., Yin, Q.-Z., Rustad, J. R., and Casey, W. H. (2014). Investigating the behaviour of Mg isotopes during the formation of clay minerals. *Geochim. Cosmochim. Acta* 128, 178–194. doi: 10.1016/j.gca.2013.12.012

Wimpenny, J., James, R. H., Burton, K. W., Gannoun, A., Mokadem, F., and Gíslason, S. R. (2010). Glacial effects on weathering processes: new insights from the elemental and lithium isotopic composition of West Greenland rivers. *Earth Planet. Sci. Lett.* 290, 427–437. doi: 10.1016/j.epsl.2009.12.042

Wunder, B., Meixner, A., Romer, R. L., Feenstra, A., Schettler, G., and Heinrich, W. (2007). Lithium isotope fractionation between Li-bearing staurolite, Li-mica and aqueous fluids: An experimental study. *Chem. Geol.* 238, 277–290. doi: 10.1016/j.chemgeo.2006.12.001

Yang, H., Konzett, J., Downs, R. T., and Frost, D. J. (2009). Crystal structure and Raman spectrum of a high-pressure Li-rich majoritic garnet, $(Li_2Mg)Si_2(SiO_4)_3$. *Am. Mineral.* 94, 630–633. doi: 10.2138/am.2009.3144

Yde, J. C., Knudsen, N. T., Hasholt, B., and Mikkelsen, A. B. (2014). Meltwater chemistry and solute export from a Greenland Ice Sheet catchment, Watson River, West Greenland. *J. Hydrol.* 519, 2165–2179. doi: 10.1016/j.jhydrol.2014.10.018

Yeghicheyan, D., Carignan, J., Valladon, M., Bouhnik Le Coz, M., Le Cornec, F., Castrec-Rouelle, M., et al. (2007). A compilation of silicon and thirty one trace elements measured in the natural river water reference material SLRS-4 (NRC-CNRC). *Geostandard. Newslett.* 25, 465–474. doi: 10.1111/j.1751-908X.2001.tb00617.x

Conflict of Interest: The authors declare that the research was conducted in the absence of any commercial or financial relationships that could be construed as a potential conflict of interest.